University of Alberta

Jarosite Occurrences in the MIL 03346 Nakhlite:
Implications for Water on Mars

by

Jason K. Hong

A thesis submitted to the Faculty of Graduate Studies and Research
in partial fulfillment of the requirements for the degree of

Master of Science

Department of Earth and Atmospheric Sciences

Spring 2012
Edmonton, Alberta

ABSTRACT

The recent discovery of the mineral jarosite ($KFe_3(OH)_6(SO_4)_2$) in the MIL 03346 martian meteorite is important because jarosite forms from acidic, oxidizing waters. Jarosite occurrences in the MIL 03346 martian meteorite were studied to characterize the mineral in-situ. Backscattered electron images and X-ray maps reveal distinct areas of jarosite occurrences in both the mesostasis and in veins cutting cumulate augite grains. Areas of alteration range from a few microns to 100 microns in length. Quantitative analyses indicate significant amounts of hydronium substitution and chemical compositions consistent with terrestrial jarosites. Synchrotron XRF was not able to determine an origin for the jarosite due to various issues involving the beam spot size and detection limits. Hydrogen isotopic analyses indicate a terrestrial origin for the jarosite, most likely a result of Antarctic weathering processes. The methods used in this study show that not all jarosite occurrences in MIL 03346 are martian in origin.

ACKNOWLEDGEMENTS

- Dr. Christopher Herd for his mentoring and patience during my masters program. His research project allowed me to work at amazing laboratories across North America, which is one of the most positive things I will take away from this entire experience.
- Dr. Ronald Cavell for his expertise with the various synchrotron radiation techniques used in my research and for accompanying me on my research trips.
- Dr. Sergei Matveev for his help collecting my electron microprobe data.
- My thesis committee members Dr. Sarah Gleeson and Dr. Tom Chacko for their criticisms and suggestions during my thesis defence.
- Renfei Feng, Robert Gordon, and Conel Alexander for their help collecting synchrotron XRF and ion microprobe data.
- My family for their continued support during my academic career, especially after I made the decision to study in Canada.
- My close friends in both Canada and the United States, for providing temporary escapes from my research/writing and making these past few years the most memorable time of my life.

TABLE OF CONTENTS

LIST OF TABLES

Table

LIST OF FIGURES

Figure

CHAPTER 1: INTRODUCTION

Martian meteorites have been extensively studied even before the scientific community discovered that they were martian. Excluding the famed ALH 84001 orthopyroxenite, all martian meteorites are classified into three groups: shergottites, nakhlites, and chassignites. They are named after the location of the first meteorite that was discovered for their respective groups and were grouped together based on their chemical, isotopic, and geological characteristics (McSween 1985). Collectively these meteorites (including ALH 84001) were originally classified as the SNC meteorites until enough evidence was collected to strongly suggest a martian origin. Today they are simply called martian meteorites.

The evidence of a martian origin for the SNC meteorites come from the studies of their volatile gas components, isotopic signatures, and geochronology. Specifically the concentrations of CO_2, N_2, noble gases and their isotopes closely match the measured concentrations of the current martian atmosphere by the Mars Viking Lander (Treiman et al. 2000). These gases are found trapped in pockets of glass that formed as a result of impact shock, perhaps during the impact event that launched the meteorites from the martian surface. These gases' relative abundances are not seen in any other volatile reservoir that has been studied and are unique to Mars and the martian meteorites (Treiman et al. 2000). The isotopic signatures of the SNC meteorites provide additional support for a martian origin. The SNC meteorites follow their own oxygen fractionation line that differs from the Earth and Moon (Clayton et al. 1983). Isotopic ratios for hydrogen reflect

much heavier ratios than seen on Earth (Meyer 2006). δD values in SNC meteorites have been shown to be as high as +4300‰ (Watson et al. 1994), far outside the standard for terrestrial waters (0‰). δD values are calculated using the following equation:

$$\delta D = 1000 \times (\frac{R\text{sample}}{\text{Rstd}} - 1)$$

Where $R = \frac{2H\ counts}{1H\ counts}$ and $Rstd = 1.5576 \times 10^{-4}$.

Sm-Nd and Rb-Sr age-dating show that the nakhlites and chassignites formed ~1.3 Ga while shergottites formed more recently at ~180-600 Ma (Nyquist et al. 2001). The relatively young ages of the SNC meteorites would require a large geologically active parent body from 1.3 Ga to 180 Ma. Combined with the much older ALH 84001 meteorite (4.5 Ga), the SNC meteorites must come from a planetary body that has surface geologic units that span the entire age of the solar system. Mars is the only terrestrial planet that meets this requirement (Treiman et al. 2000). The evidence from these studies strongly point to Mars as the only possible parent body for the SNC meteorites.

Nakhlite Background

Nakhlites are clinopyroxenites that are composed mainly of cumulate augite. Other mineral phases include minor amounts of cumulate and mesostasis olivine, and mesostasis sulfides and titanomagnetite (Treiman 2005). The titanomagnetite occurs as skeletal grains within the glassy mesostasis (Figure

1.1A). Nakhlites also contain iddingsite, a mixture of smectite clay, iron oxy-hydroxides, and salt minerals (Treiman 2005). Iddingsite, which is a result of low-temperature aqueous alteration under neutral pH, precipitates along fractures in cumulate grains and within the mesostasis. The modal mineralogies and alteration phases of representative nakhlites are presented in Table 1.1 and Table 1.2. Minor shock features are observed within the nakhlites and include undulatory extinction of augite and olivine grains, deformation twinning, and minor brecciation (Treiman 2005).

Mineral Phases in Nakhlites

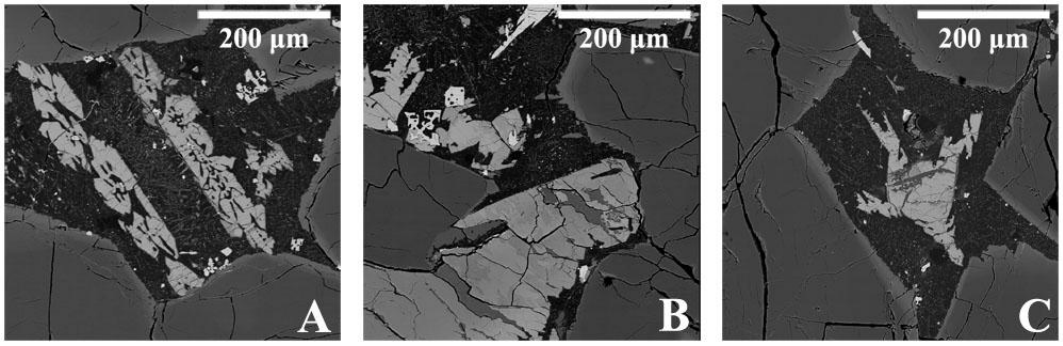

Figure 1.1: *Three BSE (backscattered electron) images and the typical mineral phases present in nakhlites (Images from MIL 03346 nakhlite). Augite grains are present in all three images as large darker grains with distinct edges. The brighter mineral phases in the centers of each image are skeletal titanomagnetite (A), cumulate olivine (B), and mesostasis olivine (C). The mesostasis shows a vitrophyric texture.*

Modal Proportions (volume %) of Nakhlites

Table 1.1:

	MIL 03346	NWA 998	NWA 817	Yamato-593	Gov. Vala.	Lafayette	Nakhla
Pyroxene	78.4	70	69	76.7	81.2	73.5	80.8
Olivine	1.1	10	12.5	12.2	8.9	16.7	10.8
Mesostasis	19.8	19	18.5	11.1	9.8	9.8	8.4

(After Day et al. 2006)

Alteration Phases in Nakhlites

Table 1.2:

	Alteration phases	Sulfides[2]
MIL 03346	Ja, Id, Sm, Ti[3]	Po
NWA 998	Id, Cal, ClAp, Pl, Kf, Ti[2]	Po,Cp
NWA 817	Sm, Si, Pl, Kf, Ti[2]	Po
Yamato-593	Ja, Id, Ti, Pl, Kf, Pi[1]	Po
Gov. Vala.	Id, Gy, glass, ClAp, Ti, Sp, Si, Pl, Kf[2]	Po,Py,Cp
Lafayette		Po,Py,Cp
Nakhla	Id, Cb, Ha, Sm, Fa, ClAp, Pl, Kf, Ti[2]	Po,Py,Cp

Notes: Cal = calcite; Cb = carbonate; ClAp = chlorapatite; Cp = chalcopyrite; Gy = gypsum; Ha = halite; Id = iddingsite; Ja = jarosite; Kf = K-feldspar; Pi = pigeonite; Pl = plagioclase; Po = pyrrhotite; Py = pyrite; Si = pure silica phases; Sm = smectite; Sp = spinel; Ti = titanomagnetite and ilmenite.
[1]Noguchi et al. (2009); [2]Chevrier et al. (2011); [3]Day et al. (2006)

Aqueous alteration in the nakhlites is most likely preterrestrial based on a few observations. There are instances where the iddingsite has been melted by the fusion crust that forms on the outside layer of the meteorite during the rapid entry into Earth's atmosphere. This indicates that the iddingsite must have been formed

before the meteorite landed on Earth (Treiman et al. 1993). Using Rb-Sr and Ar-Ar isotopic data, the formation of aqueous alteration products (iddingsite) was determined to have occurred ~620 Ma (Misawa et al. 2005, Swindle et al. 2000), which would require a parent body with an active groundwater system at that time (Treiman 2005).

Stable isotope analysis of the iddingsite in the Lafayette nakhlite yielded non-terrestrial isotope ratios (Romanek et al. 1998). Oxygen isotopic ratios of the iddingsite in Lafayette were measured by Romanek et al. (1998) and found to have enrichments in ^{17}O, resulting in oxygen ratios that lie above the terrestrial mass fractionation line. Interestingly, the iddingsite's $\Delta^{17}O$ value is higher than the magmatic phases (olivine and pyroxene), which suggests that the crustal fluids on Mars represent a different component, distinct in composition from the igneous portion. Romanek et al. (1998) suggests that the fluid reservoirs on Mars contributing to the formation of iddingsite were isotopically altered through exchange with atmospheric components. This scenario implies a connection between the fluid reservoir and the atmosphere which determine the isotopic ratios of the later aqueous alteration products.

A brief geologic history of the nakhlites is presented by Treiman (2005). Accumulation of pyroxene and olivine began in a magma chamber containing the nakhlite parent magmas. The nakhlites then cooled and crystallized at roughly 1.3 Ga. The rock was then altered by liquid water to form iddingsite at around 620 Ma. The nakhlites were then ejected from Mars by an impact event which sent

them into orbit for 10 million years (determined by cosmic ray exposure ages) before finally landing on Earth as meteorites (Nyquist et al. 2001).

The nakhlite suite of martian meteorites provides a critical piece in the reconstruction of Mars' past. The limited collection of martian meteorites represents the large gap in the rock record of Mars. These gaps demonstrate the importance of studying alteration products and the processes that formed them after the rock crystallized on Mars. Most importantly, the occurrence of aqueous alteration products in the nakhlites provides evidence for the activity of water near the martian surface.

MIL 03346 Background

The MIL 03346 nakhlite was found in the Miller Range of Antarctica on December 15, 2003 with a total of 715 grams recovered (Figure 1.2). The terrestrial residence age of the MIL 03346 nakhlite has not yet been determined.

Photographs of MIL 03346

Figure 1.2: *Photographs of collected pieces of MIL 03346*

(After C. Meyer 2008)

The MIL 03346 nakhlite's cosmogenic exposure age (the time spent traveling in space) of 9.5 m.y. is similar to the other nakhlites. This age was determined by measuring changes in the isotopic ratios of noble gases, which are affected by exposure to cosmic rays (Day et al. 2006). The crystallization age of the MIL 03346 nakhlite was also determined to be similar to the other nakhlites by using Rb-Sr and Sm-Nd isotopic studies (Shih et al. 2006). The modal proportion of minerals in MIL 03346 is also very similar to the other nakhlites (Table 1.1).

Despite MIL 03346's similarity to the other nakhlites, a few unique characteristics distinguish MIL 03346 from the group. Although the augite proportion is consistent with the other nakhlites, the abundances of olivine and mesostasis stand apart. MIL 03346 has a much lower abundance of olivine but a higher abundance of mesostasis. The evidence for rapid cooling in the MIL 03346 nakhlite is provided by the high volume percentages of glass and skeletal mineral phases, as well as the lack of plagioclase laths present in other nakhlites (Day et al. 2006). The differing modal mineralogy of the MIL 03346 nakhlite is not the only reason for its significance among the suite of nakhlites. The importance of the MIL 03346 is defined by its multiple occurrences of jarosite in addition to the commonly observed iddingsite. The significance of this aqueous alteration mineral in the MIL 03346 nakhlite is discussed in detail later in the chapter.

The cooling history of the MIL 03346 nakhlite is represented by the textures of the mineral phases. For example, the quenched texture of the olivine and the vitrophyric texture is indicative of a large contrast in temperature between

the melt and the environment where the rock crystallized (Day et al., 2006). Day et al. (2006) also suggested that the low abundance of olivine in the MIL 03346 nakhlite might be due to olivine crystal sorting that occurred during the crystallization of the nakhlite in the magma chamber.

Day et al. (2006) studied the petrology and chemistry of the MIL03346 nakhlite in detail. The composition of the augite and olivine grains show a dominant trend of relatively Mg-rich cores, zoning to very Fe-rich rims (Figure 1.3).

Olivine and Augite Compositions in MIL 03346

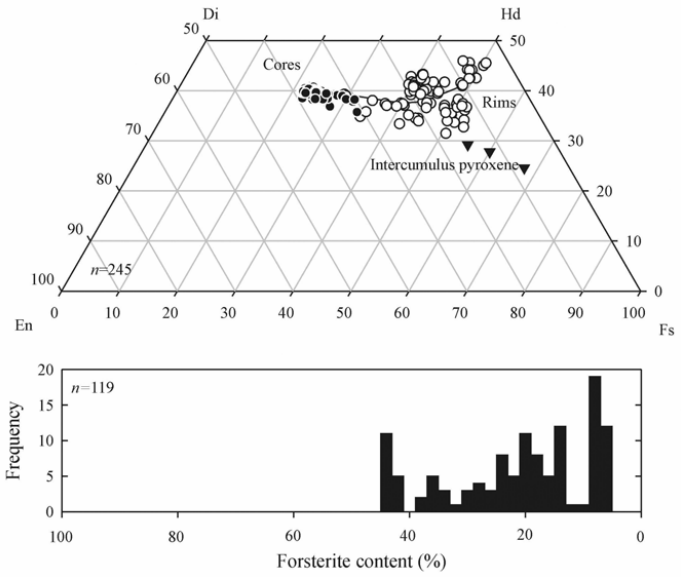

Figure 1.3: *Olivine (bottom) and augite (top) compositions in MIL 03346*

(After Day et al. 2006)

The aqueous alteration of iddingsite in the MIL 03346 meteorite has similar elemental concentrations as the other nakhlites, which indicates consistent fluid activity in the original nakhlite body (Day et al. 2006). Rare earth element concentrations for the MIL 03346 intercumulus glass and nakhlite whole rock are shown in Figure 1.4. In general, all nakhlites are enriched in LREE and show similar REE patterns which provides supporting evidence for the possibility that all the nakhlites originated from a common magma chamber.

Rare Earth Element Patterns for MIL 00346

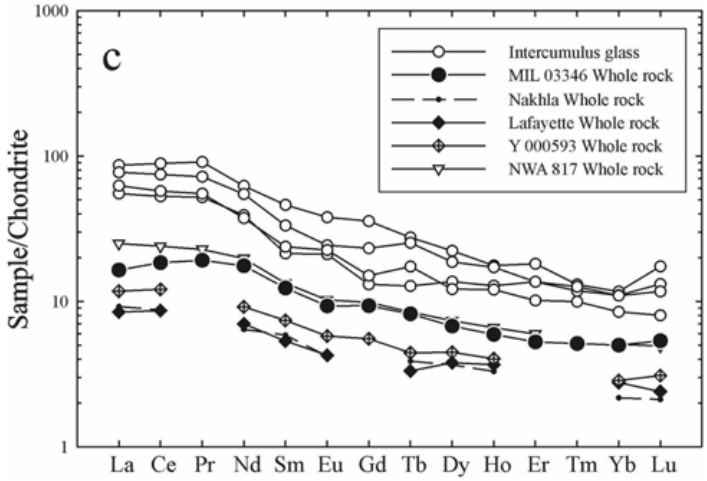

Figure 1.4: *Chondrite-normalized REE patterns for intercumulus glasses and MIL 03346 whole rock compared to other nakhlites.*

(After Day et al. 2006)

Jarosite in MIL 03346

The recent interest to identify the relationships between nakhlites and the mineral jarosite [$KFe^{3+}_3(SO_4)_2(OH)_6$] began with the discovery of jarosite veinlets

within a sample of the MIL 03346 nakhlite (Herd 2006). This observation followed the discovery of jarosite on the surface of Mars by the Mars Exploration Rover (MER) *Opportunity* (Klingelhöfer et al. 2004). To date, jarosite has only been discovered in one other nakhlite, Yamato-593 (Noguchi et al. 2009). These recent developments have initiated new research to determine the potential importance of the jarosite found in martian meteorites. The ability to study jarosite within a martian thin section in detail is something remote sensing equipment cannot reproduce. The tools in laboratories today are able to provide quantitative information on micron-scale features like the jarosite found in MIL 03346. Since jarosite is found both on Mars by the MER and in the nakhlites, the temptation exists to assume that the nakhlite jarosite is martian. However, firm evidence has yet to be presented in support of a martian origin.

The discovery of jarosite is significant because of the specific environmental conditions required for its formation. In terrestrial occurrences of jarosite, the mineral is associated with a wet, acidic, and oxidizing environment (Papike et al. 2006). The presence of jarosite in the MIL 03346 nakhlite implies that the near-surface of Mars must have experienced similar geochemical processes as those seen on Earth. Assuming the jarosite formed on Mars, evidence for aqueous alteration by martian near-surface waters is supported by the enrichment of deuterium in alteration products in younger martian meteorites; this enrichment is due to the preferential loss of hydrogen to space (Greenwood et al. 2007). The possibility of a closely related environment for jarosite formation on

Mars requires further characterization of the jarosite found in the MIL 03346 nakhlite.

An occurrence of jarosite was discovered in specimen MIL 03346, 165 by Herd (2006). That study used electron microprobe X-ray mapping followed by Raman spectroscopy and ToF-SIMS to confirm the presence of jarosite. The jarosite crosscuts the iddingsite which could indicate that the altering waters shifted from neutral to acidic assuming the jarosite formed on Mars. The area of alteration is on the scale of microns.

Other studies have been done on different sections of the MIL 03346 nakhlite with similar results. Vicenzi et al. (2007a,b) used a combination of electron microprobe, Raman spectroscopy, and ion microprobe to analyze the jarosite found in the MIL 03346 nakhlite. The study identified veinlets of goethite later filled by jarosite, again supporting the possibility of a change in pH of the altering waters from neutral to acidic. Backscattered electron imaging and X-ray mapping revealed that the jarosite occurs in veins that range in width from sub-micrometer up to ~10 micrometers. BSE images reveal that at least one jarosite vein crosscuts the fusion crust, which would indicate that some degree of aqueous alteration must have taken place in Antarctica. Raman imaging results shows that Na or hydronium substitutes in for the K for the majority of the jarosite (Vicenzi 2007b). These studies were unable to determine if any part of the fusion crust crosscuts the jarosite as voids typically occupy the space between the fusion crust and the jarosite-filled veins.

Vicenzi et al. (2007a) analyzed the hydrogen isotopic compositions of jarosite in the MIL 03346 nakhlite. An ion microprobe was used to spot analyze the jarosite found in a thin section of the meteorite. The δD values range from 2498 ± 480 ‰ to 2956 ± 955 ‰, which is outside the range for terrestrial waters. The δD values for other martian meteorites range from -150 to +4300 ‰ (Watson et al. 1994). This range is much larger than the range for δD of water on Earth (-480 to +130 ‰; Hoefs 2004). The wide range of hydrogen isotopic compositions seen in the martian meteorites could be caused by either the mixing of a martian atmospheric component with martian magmatic water or from terrestrial water contamination (Vicenzi et al. 2007a).

Jarosite was also found in a melt inclusion within a pyroxene grain, which may have been hydrothermally precipitated on Mars (McCubbin et al. 2009). This is a unique occurrence that implies that high temperature magmatic fluids played a role in precipitating at least some jarosite in MIL 03346. McCubbin et al. (2009) suggests that all the necessary components required to precipitate jarosite were present in the melt inclusion at a temperature above the thermal stability of jarosite (~200°C). The melt inclusion was then stable enough to precipitate jarosite once the fluids cooled.

Environments of Jarosite Formation

Papike et al. (2006) provides models for the formation of terrestrial jarosite in three types of environments: supergene, sedimentary, and steam-heated (Figure 1.5). For supergene and steam-heated jarosite to form, a few things must occur beforehand. First, SO_2 and H_2S originating from the shallow crystallizing

magma must be oxidized to provide the acidic fluids required for jarosite to form. Second, water and SO_2 must react to produce H_2S and H_2SO_4, followed by oxidation of the H_2S, which would provide the low pH needed for jarosite to be the stable phase. The difference between supergene and steam-heated jarosite is dependent on the species that is oxidized. Supergene jarosite results from the oxidation of pyrite while steam-heated jarosite results from the oxidation of H_2S. On Earth, atmospheric oxygen provides the oxidizing agent whereas on Mars, the most likely oxidation mechanism is the reduction of atmospheric CO_2 to CO due to Mars' low atmospheric oxygen content (Papike et al 2006).

Environments of Jarosite Formation

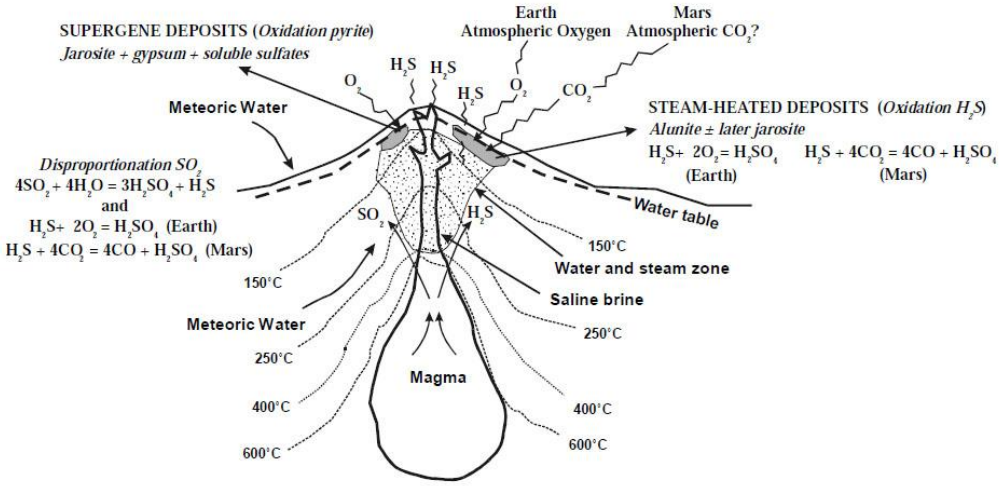

Figure 1.5: *Jarosite formation models for three different environments.*

(After Papike et al. 2006a)

The third environment is sedimentary jarosite, requiring acid-saline lakes where the mineral is precipitated within the near-surface sediment. The source of the sulfate could be from wind-blown sulfate aerosols originating from neighboring seawater (Alpers et al., 1992).

Meridiani Planum's environment contains sediments which include abundant hematite and sulfate minerals. These were possibly deposited in episodic events of shallow bodies of briny water, with evaporation resulting in the precipitation of sulfate minerals (Squyres et al. 2004). Others have proposed that the area experienced deposition of volcanic ash which reacted with SO_2 during diagenesis of the bedrock, an environment which could occur at high temperatures and would not require long-standing bodies of water (McCollom et al. 2005).

Experimental studies of jarosite stability have shown that jarosite is more stable with decreasing temperatures., and that increasing temperatures favors the Na end-member (Stoffregen 1993). On Mars, the low temperature of the planet's surface does not immediately indicate that jarosite is stable there. Since Mars has a much lower pressure than Earth, (6 mbar [Kliore et al. 1965] vs ~1000 mbar respectively), thermodynamic calculations were done by Navrotsky et al. (2005) to determine the equilibrium decomposition temperature for jarosite on the martian surface. They found this temperature to be 18° C, which is lower than most latitudinal and seasonal tempertures reported for the martian surface (Kieffer et al. 1977). Navrotsky et al. (2005) concluded that jarosite is thermodynamically stable under normal conditions on the present martian surface (Figure 1.6)

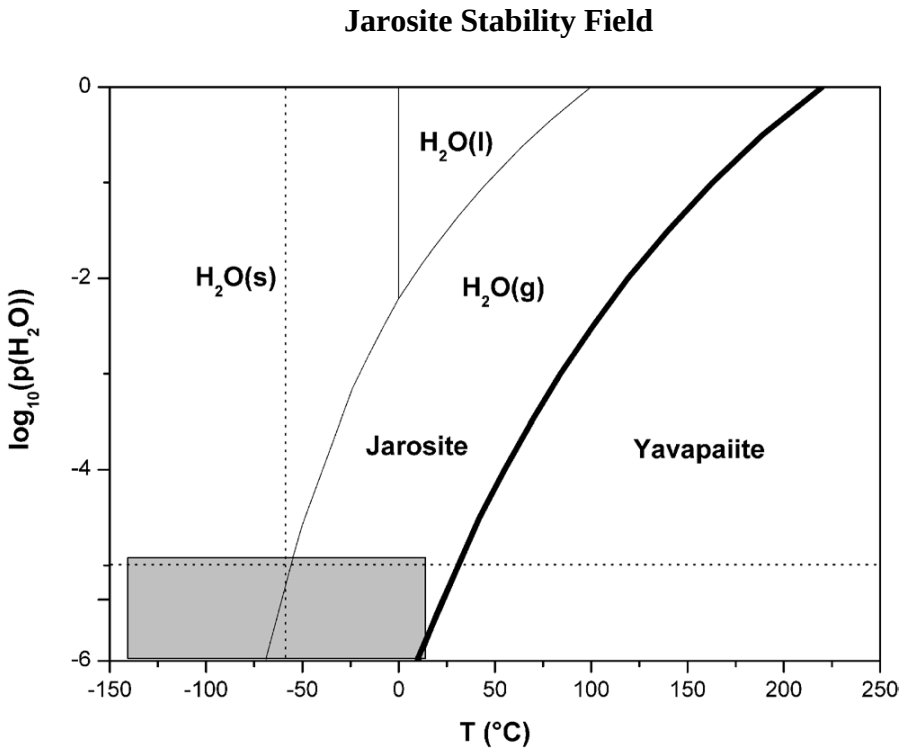

Figure 1.6: *Stability field of jarosite under martian pressure and temperature conditions. Grey area represents normal surface conditions on Mars at Meridiani Planum. Overlap of grey area and jarosite stability field indicates that jarosite is stable under normal conditions on the martian surface.*

(After Navrotsky et al. 2005)

Geologic Setting of Jarosite Standards

In this study, two terrestrial jarosites are used as standards for direct comparison with the jarosite occurrences in the MIL 03346 nakhlite. The localities of these terrestrial jarosites have previously been studied as possible Mars analogue sites (Fleisher et al. 2008, Burger et al. 2007). The first terrestrial jarosite standard is from the Pena Blanca District in Mexico. This is a hydrothermally-deposited jarosite and is characterized by coarse, euhedral

crystals (Figure 1.7). The jarosite crystals are commonly associated with fluorite within rhyolite breccias (Lueth et al. 2005) and were formed in fluids at 180°C (Goodell et al. 1999). The second jarosite standard is from Barranco del Jaroso, Spain. This jarosite is the world locality type and occurs in the Jaroso Ravine of the Sierra Almagrera. This jarosite has hydrothermal origins associated with supergenic episodes of sulfate precipitation (Rull et al. 2010) at fluid temperatures between 150° and 360°C (Martinez-Frias et al. 2004). These samples typically occur as clusters of tabular crystals (Figure 1.7) associated with amorphous Fe-oxides (Desborough et al. 2010).

Photographs of Terrestrial Jarosites

(Photo by: Rob Lavinsky) (Photo by: Frédéric Hède)

Figure 1.7: *Left: Pena Blanca jarosite; Right: Barranco del Jaroso jarosite (images from mindat.org)*

Synchrotron Radiation in the Study of Martian Meteorites

Synchrotron radiation has been used to study iddingsite veins in other nakhlites. In Noguchi et al. (2009), the Yamato 00 nakhlites were studied using synchrotron XRD. Diffraction peaks of features as small as 5 micron in width were able to be detected using this method. Noguchi et al. (2009) were able to distinguish the iddingsite using diffraction peaks from laihunite and jarosite, although they were not able to find peaks for the minor iron oxyhydroxides due to poor crystallinity. Synchrotron XRF was carried out by Herd (2006) on a jarosite occurrence within a mesostasis olivine grain. using a 4 x 4 micron spot size at ID-20, PNC-CAT at the Advanced Photon Source, which produced K and Fe maps comparable to those obtained by electron microprobe, as well as maps of Rb, Sr, and Zn.

Terrestrial Analogs: REE chemistry

Studies of trace element compositions are a powerful tool in understanding a variety of geochemical processes (e.g., Burger et al. 2009). For instance, REEs are more soluble in acidic solutions, providing information on the fluid origin and evolution (Humphris 1984). The trace elements of particular interest in jarosite are V, Ce, and Eu as these multivalent elements are able to trace changes in pH and fluid chemistry (Burger et al. 2009). For example, cerium has the ability to constrain the pH under which the jarosite precipitated as Ce^{3+} is stable in a lower pH while the stability of Ce^{4+} increases with higher pH. Vanadium could be used to determine fluid redox conditions (i.e. degree of oxidation). All terrestrial

jarosite samples studied by Burger et al. (2009) showed slightly positive Eu anomalies. This study measured the capabilities of synchrotron XRF methods in determining trace element compositions.

Purpose of Study

The goal of this project was to characterize the jarosite in the MIL 03346 nakhlite in two different specimens using a range of methods. Electron microprobe was used to provide initial information about the specimens via X-ray mapping and quantitative analysis of the jarosite alteration. Synchrotron radiation techniques were applied to the jarosite to assess the current capabilities of synchrotron XRF in providing quantitative trace element data. Ion microprobe techniques were used to determine if the jarosite is martian or terrestrial as indicated by δD values.

CHAPTER 2: METHODS

Sample Preparation

Two MIL 03346 (MIL 03346, 165 and MIL03346, 190) thin sections were provided by NASA for this study and required no sample preparation. The specimens are mounted on one inch quartz rounds with a polished epoxy layer covering the sample surface (Figure 2.1).

Thin Section Scans of MIL 03346 Specimens

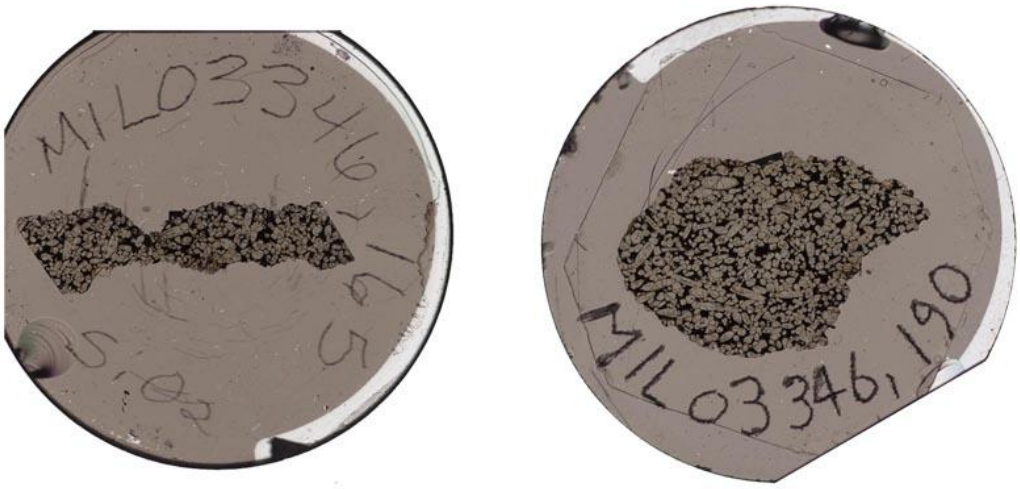

Figure 2.1: *Left: MIL 03346 ,165; Right: MIL 03346 ,190.*

The two terrestrial jarosite samples (Pena Blanca and Barranco del Jaroso) were prepared simultaneously using the same process. A portion of each sample was placed into a one inch round puck using Petropoxy 154. The process mounts the sample by combining an epoxy resin and a curing agent in a 10:1 ratio respectively. The mounts were cured in a vacuum overnight to prevent the

formation of air bubbles. Air bubbles near the sample can result in a weaker mount which can cause pieces of the sample to pluck out during the polishing process. Each epoxy puck was polished to expose the sample surface using an alumina (Al_2O_3) polishing compound. Samples were polished using polishing plates of varying grit (10 µm, 5 µm, 0.05 µm) coated with a mixture of water and the alumina compound. The plates were placed in a varying speed wheel which is controlled by the user. The length of this process depends on the hardness of the sample. Softer samples required longer polishing times as extra precaution was needed to prevent pieces of the specimen from plucking out of the epoxy. After polishing, the mount was put under an optical microscope to ensure a clean and polished specimen surface.

Optical microscopy

Prior to any optical microscopy, high resolution thin section scans of both MIL 03346 specimens were taken at the Digital Imaging Facility (University of Alberta) using a Nikon Super Coolscan 5000 ED thin section scanner. Printouts of these scans are used as maps for this study (Figure 2.1.).

Areas of alteration in the two MIL 03346 thin section samples were found using transmitted-light optical microscopy (10x magnification), by locating areas of rust-coloured staining within the thin section. The presence of aqueous alteration does not necessarily indicate jarosite precipitation but instead they more likely represent areas of iddingsite, the major aqueous alteration phase in the MIL nakhlites (Treiman 2005). Optical microscopy is therefore most useful for locating all areas of interest for later electron microprobe analyses. Aqueous

alteration was most noticeably found within the mesostasis or intercumulus areas, but also occurred in veins cutting through cumulate augite and isolated olivine grains. Between the two thin sections, 30 areas of alteration were initially selected to be analyzed further using EPMA (17 from MIL 03346, 165, and 13 from MIL 03346, 190)

Reflected-light optical microscopy was used to locate sulfide grains and Fe-oxides within the mesostasis. The locations of these grains were used to determine their relationships with the jarosite occurrences.

Electron Microprobe

MIL 03346 Samples:

The areas of alteration located using optical microscopy were studied in detail using a Cameca SX-100 electron microprobe. The beam source was set to 20 keV and 10 nA with a dwell time of 15 ms. Both thin sections were carbon coated prior to microprobe analysis and loaded into the sample holder simultaneously. Using the areas of interest located by optical microscopy, BSE images were obtained and waypoint coordinates were stored in the operating software for the Cameca in order to set up the X-ray maps. Each microprobe session had an allotted time of 24 hours which required X-ray maps to be prioritized based on results from BSE imaging of the areas of interest.

Prior to X-ray mapping, the electron microprobe was used to quantitatively analyze the preselected areas of aqueous alteration for their elemental compositions. Quantitative measurements of weight percent oxides of the major elements in jarosite (Na, K, Fe, S) were taken using both spot and line

analysis, when possible. Other minor elements (Al, Mg, Cr, Mn, P, Si, Ti) were also quantitatively measured.

The jarosite compositions for the MIL 03346 jarosite occurrences and the terrestrial jarosites were determined stoichiometrically by using the ideal jarosite formula [$A_1M_3T_2O_8Z_6$] normalized to 14 anions. Each site is allocated as follows: A-site (K, Na, hydronium as H_3O), M-site (Fe, Al, Mg, Cr, Mn), T-site (S, P), and Z-site (hydrogen as OH). The hydrogen content was stoichiometrically calculated to completely fill the Z-site as OH. In addition, any remaining space in the A-site was filled as hydronium. The weight total was then verified to be close to 100% after including the calculated H content. The formula recalculation of the MIL 03346 jarosite occurrences is more complicated than the process used with the terrestrial samples. Since the MIL 03346 jarosite is not homogeneous, other intergrown phases interfere with the analyses. In order to correct this, these other phases were subtracted from each analysis before calculating the jarosite formula. In most cases, this process resulted in weight totals close to 100%. Since the terrestrial jarosite samples contained large areas of pure jarosite, the linear subtraction method was not required.

Stage scan X-ray mapping of K, S, Fe, Si, and Al was done to locate and image the jarosite. All X-ray maps had corresponding BSE images taken for reference and later image processing and presentation. All X-ray maps taken had an area of 500 x 500 µm and a step size of 1 µm. The high resolution of the maps provided enough detail to distinguish the various phases from one another. The large areas also allowed for qualitative interpretations on the mode of jarosite

precipitation by observing the relationships between the jarosite and the surrounding mesostasis and cumulate grains.

The standards used for the quantitative analysis and X-ray mapping were orthoclase (K), hematite (Fe), sphalerite (S), pyrope (Al), diopside (Si), albite (Na), garnet (Mg), Cr_2O_3 (Cr), spessartine (Mn), apatite (P), garnet (Si), and rutile (Ti).

Terrestrial Samples:

The two terrestrial samples were analyzed using a similar process as was used for the MIL 03346 samples. BSE images were taken and quantitative analysis was done on the Pena Blanca sample. Both quantitative analysis and X-ray mapping were done for the Barranco del Jaroso sample.

Image Processing

The resulting X-ray maps were processed using the ImageJ program (ImageJ is a Java-based image processing program that is adaptable for a wide range of applications due to its user-written plugins and macros). To reveal areas of jarosite alteration, image operators in the ImageJ software were used on the elemental maps for K, S, and Fe (K AND S AND Fe function). The resulting image isolates areas where K, S, and Fe occur together, which were interpreted as locations of jarosite, and later verified by quantitative analysis. The processed images were overlain onto the corresponding BSE images to study the setting of

the jarosite in relation to the host rock. The resulting composite images allow for a qualitative assessment on the mode of jarosite precipitation.

Synchrotron Radiation Methods

Synchrotron radiation is the electromagnetic radiation that is emitted when electrons travelling near the speed of light are bent by an external magnetic field in a particle accelerator (Elder et al. 1947). Synchrotron radiation provides a higher flux (number of photons per second), brightness (flux per vertical angle), and brilliance (brightness per source area) when compared to traditional X-ray sources (Blanchard 2011).

Synchrotron XRF analysis was chosen because the method potentially suited the goals of this study. Since the samples are limited to thin sections containing micron scale jarosite occurrences, only instruments with high special resolution like the electron microprobe are potentially useful. Synchrotron XRF has a spatial resolution smaller than 5 μm and is also non-destructive, which is advantageous when studying martian meteorite samples, as this allows for repeated measurements within the same area of the sample without a loss of signal. The objective of synchrotron XRF was to quantitatively determine the trace elements for both the MIL 03346 and terrestrial jarosite. The goal was to compare the MIL 03346 jarosite directly to the terrestrial jarosite to see if any differences exist between their minor element compositions and if those differences can show that the MIL 03346 jarosite is martian in origin. Both light

sources used in this study also have the option to analyze the jarosite structure in addition to its elemental composition.

Two third generation light sources were used to obtain synchrotron XRF data. Third generation light sources have been built since the early 1990's. They are characterized by a lower electron beam emittance, high currents, and high brightness (photon flux) when compared to previous generations of light sources. The third-generation synchrotrons today include many end stations consisting of either an insertion device (ID) or a bend magnet (BM) section. For reference, first-generation rings were used specifically for high energy physics research and second generation rings were built as actual light sources for more expanded applications by maintaining the electrons in an ultra-high vacuum storage ring. Insertion devices (the type of end station used for this study) were not a common feature of synchrotrons until the third generation light sources were built. Insertion devices consist of a series of magnets that are added to the straight sections of the storage ring. Their purpose is to increase the brightness and brilliance of the X-ray beam. Insertion devices are able to focus the beam in the storage ring back to its smallest possible dimensions, resulting in spot sizes smaller than 5 microns. For this reason, insertion devices are the preferred source point for synchrotron microprobes.

Magnets with alternating polarity force the electrons into a sinusoidal flow that result in pulses of radiation that are out of phase. Constructive interference produces narrow peaks with higher brightness. The increased brightness allows for faster collection of high resolution data.

Canadian Light Source and VESPERS:

The Canadian Light Source (CLS) is a 2.9 GeV synchrotron located in Saskatoon, Saskatchewan. The VESPERS (Very sensitive Elemental and Structural Probe Employing Radiation from a Synchrotron) beamline was used for this study. VESPERS was chosen because of its high special resolution (2-4 μm) and its ability to perform XRF and XRD measurements simultaneously. The VESPERS beamline primary beam is a polychromatic or "pink" beam which provides fast acquisition rates and low limits of detection.

Advanced Photon Source and XOR/PNC-ID:

The Advanced Photon Source (APS) is a 7 GeV synchrotron located within the Argonne National Laboratory in Chicago, Illinois. The higher energy output of this facility provides a beam that is potentially brighter than what is possible at the CLS while maintaining the ability to perform XRF and XRD measurements simultaneously. The XOR/PNC-ID beamline used at this facility is able to provide a spatial resolution of 3-5 μm and is very similar to the capabilities of the VESPERS beamline.

At the VESPERS beamline, the sample holder is angled 45 degrees from both instruments in order for the Vortex 4-element detector (XRF) and CCD imager (XRD) to obtain data simultaneously (Figure 2.2). The samples themselves are taped to the sample holder which has a magnetized base that attaches to the sample stage. This allows the user to preserve the coordinates (to within a micron) for where the beam is contacting the sample surface, even when

samples are being swapped back and forth. This is an advantage unique to the VESPERS beamline and the CLS. The XOR/PNC-ID beamline does not share this advantage for sample switching.

The XOR/PNC-ID beamline hutch setup is similar to the VESPERS beamline. The sample holder is angled 45 degrees from the horizontal with the Vortex 4-element detector mounted 90 degrees with respect to the incoming beam. The CCD imager is located behind the sample mount directly in line with the beam. The sample holder is attached to the sample stage by a set of screws. While this setup does secure the sample well, any switching between different thin sections does not preserve the coordinates used for locating the beam on the sample surface.

Diagram of Beamline and Sample Setup

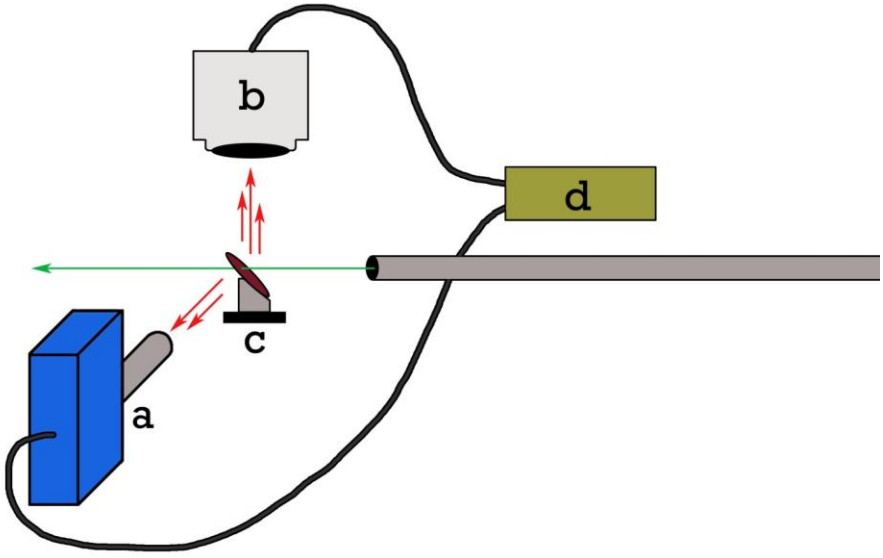

Figure 2.2: *a. Vortex-ME4 detector (XRF), b. CCD detector (XRD), c. Specimen and holder, d. Computer*

Both beamlines use the Vortex-ME4, a four-element silicon drift detector (SDD) X-ray detection system. The detector offers a high energy resolution and high throughput performance to minimize the dead time between each analysis. The detector is also able to provide fast X-ray mapping. The exceptional capabilities of these particular detectors are ideal for many applications not only limited to geologic studies.

Beam Settings for APS and CLS

The APS analyses used a mono beam set to 13 keV with a beam size of 3-5 microns. The CLS analyses used a poly (variable) beam with an energy range of 4-30 keV, although the analysis was only effective to 20 keV as the response of the detector decreased beyond 20 keV. The beam size at the CLS is 2-4 microns.

Micro-XRF Sample Analyses

Both beamlines used a similar setup for synchrotron XRF analyses. The CLS uses a Linux based software while the APS uses Windows software. Regardless of the operating system, the general process does not differ between the two beamlines since they are both using the same XRF detector. The Vortex 4-element detector allows the user to set up to 16 energy ranges of interest (ROI). Ideally each of these ROI's would represent a specific element. The detectors also allow the user to drop in filters to attenuate very high signals that can potentially flood the counting mechanism of the detector. This is especially useful for analyzing jarosite since the Fe signal may overwhelm other elements present at the same location. The process for producing synchrotron XRF maps is similar to

X-ray mapping using the electron microprobe. The user is able to set the size of the map and the coordinates.

Analysis Setup of Typical Range of Interests

Table 2.1:

	Energy		
	Low (eV)	High (eV)	ROI Name
ROI 0	6250	6550	Fe-Ka
ROI 1	3250	3400	K-Ka
ROI 2	4850	5150	V-Ka
ROI 3	5800	6000	Mn-Ka
ROI 4	4500	4700	Ti/La-Ka
ROI 5	3600	3800	Ca-Ka
ROI 6	8370	8790	Zn-Ka
ROI 7	10230	10620	As-Ka
ROI 8	7800	8190	Cu-Ka
ROI 9	6780	7290	Fe-Kb
ROI 10	5250	5550	Cr-Ka

The ranges of interest (Table 2.1) were determined by doing a test run with the sample in place and with the beam centered over a jarosite vein. All visible lines from the resulting analysis were given their own energy range to be quantified in the experimental runs. The minor elements that were not visibly detected during the test run (e.g. Vanadium) had their energy range of interest manually entered into the program in the event that longer analyses would yield quantifiable amounts.

As synchrotron XRF maps take longer than X-ray maps to complete, the size of the maps had to be varied to get the most data from the allotted beamtime.

Map sizes varied from 50 x 50 µm to 600 x 600 µm. The difficulty of synchrotron XRF is locating the beam on the sample surface. The weak optical microscope within the hutch is not comparable to the resolution of a BSE image from the microprobe. To ensure that the synchrotron XRF maps were targeting the areas of interest, a survey map was taken prior to each high resolution map. Typically a survey map would use a step size of 10-20 µm and a scan area of 500 x 500 µm. Using the survey as a guide, new coordinates would be set up with a smaller, higher resolution map (100-200 µm) at a smaller step size of 3-5 µm.

Due to the process of focusing the incoming beam, the shape of the synchrotron light is not circular but instead elliptical. To take advantage of the smaller vertical component of the beam, the sample was orientated in a manner that would benefit the areas of interest. An example is shown in the BSE image in Figure 2.3. The white arrow represents how the thin section was positioned in the sample holder. Orientating the beam this way allows for the highest resolution when positioned directly on the jarosite vein and also minimizes the possible interference from the neighbouring augite grains during analysis.

Beam and Sample Positioning

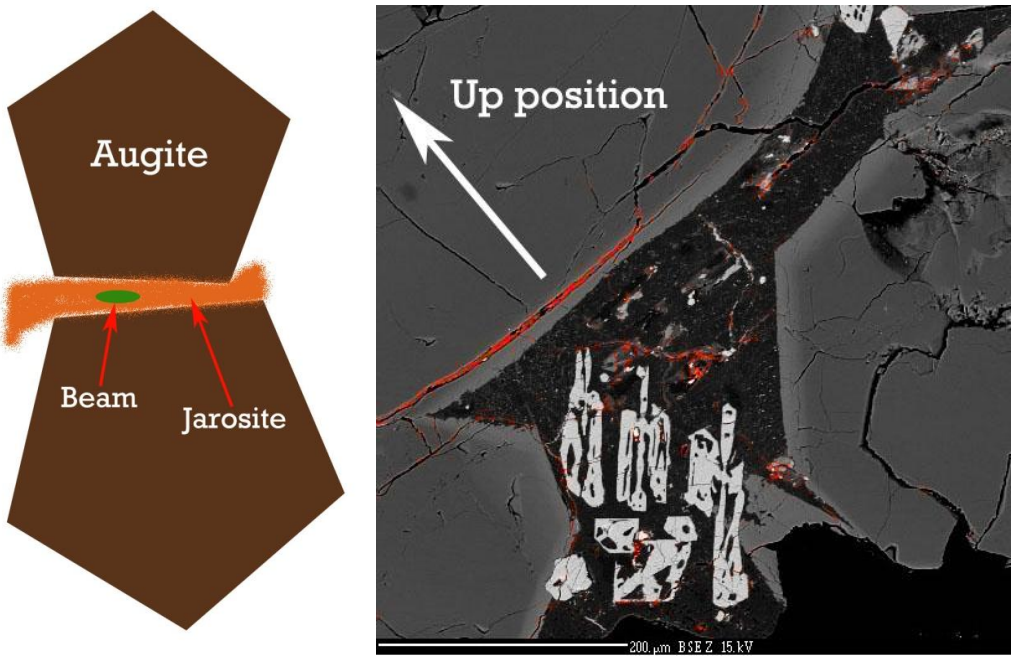

Figure 2.3: *Left: Ideal positioning of sample and beam for highest resolution; Right: Jarosite represented by falsely-coloured red.*

Quantitative Analysis of Micro-XRF Spectra:

The goal of the XRF analyses was to remove the background and fit peaks for each trace element of interest. The intensities of the peaks were used to estimate the relative concentration of each element compared to the terrestrial jarosite standards (Pena Blanca and Barranco del Jaroso). Hansteen et al. (2000) determined that detection limits for trace elements are in the order of 1 to 10 ppm and have a precision of better than 1% (expressed as standard deviation/mean x 100). Calculations for quantitative elemental concentrations in the MIL 03346

jarosite are possible only if trace element peaks are distinguishable from the background noise.

Beamline Differences

The major difference between the two light sources in this study comes from the handling of the storage rings. At the CLS, the storage ring is reinjected with electrons every 12 hours. This is different from the APS which uses a top-up method to constantly keep the storage ring at max capacity by continuously injecting lost electrons. However, these differences do not significantly affect the measurements in the samples; they only change the planning process of the analyses at the CLS, as appropriate time management of larger XRF maps is required to work around the short downtime of the beam every 12 hours.

Ion Probe

Previous studies have measured hydrogen isotopes in MIL 03346 and provided evidence for preterrestrial origins (Vicenzi et al. 2007a). For this study, the MIL 03346 samples were analyzed using the Cameca IMS 6f ion probe at the Carnegie Institution in Washington, D.C. The Cameca IMS 6F used a cesium beam with a primary beam current of 0.1 -1.0 nA. A primary accelerating voltage of 1.749 V and a secondary accelerating voltage of 5000 V were used for the analyses.

A polished probe mount of the terrestrial Tintic jarosite, provided by E. Vicenzi was used as a standard. This standard comes from the Tintic mining

district of Utah and is a homogeneous, supergene jarosite. The δD value of the Tintic jarosite was previously found to be ~ -600‰ (Vicenzi, 2011, personal communication). The Tintic sample and the two MIL 03346 specimens were carbon-coated before loading into the sample holder. The sample holder is only able to hold one sample at a time. The sample chamber is pumped down overnight (at least 8 hours) to ensure a very high vacuum. Each run in this ion probe study analyzed the same 5 element isotopes (Table 2.2). Precision of measurements were calculated using the standard deviation.

Elements for Isotopic Analysis

Table 2.2:

Elements	*Masses*
1H	1.007825
2H	2.014000
13C	13.003355
30Si	29.973770
34S	33.967866

The first sample to be analyzed was the Tintic standard. To remove the surface contamination from the area of interest, the beam was allowed to pre-sputter the surface for 600 seconds. The duration of pre-sputtering was determined by taking periodic measurements of the sample to observe any variations in isotope concentrations. Ten sets of measurements were taken for each location on the Tintic sample. Three locations were selected to get an

average isotope measurement. All locations yielded similar measurements for hydrogen and deuterium.

The MIL 03346 sample required more cautious pre-sputtering due to the low amount of jarosite present in the veins. The ideal pre-sputtering time was determined to be 120 seconds. This duration of pre-sputtering was a balance between having consistent measurements and preserving the jarosite as best as possible. In certain cases, even 120 seconds of pre-sputtering resulted in isotope concentration dropping significantly due to the destruction of the jarosite. Due to the destructive nature of ion probe analysis, only the largest jarosite veins in the MIL 03346 specimen were measured. The beam was reduced to a spot size of 3-4 μm to prevent any contamination to the measurements from neighboring pyroxene grains. A maximum 10 sets of measurements were taken for each area of interest. In some cases, the ion concentration dropped considerably before the last measurement, again due to the limited amount of jarosite material. In addition to analyzing the jarosite occurrences found in this study, measurements of hydrogen isotopic ratios were also taken in the occurrence previously found by Herd (2006).

In addition, isotope maps were taken of the jarosite occurrences in the MIL 03346, 165 thin section. All areas of interest were 100 x 100 μm in size and scanned for the same 5 isotopes used in the isotopic analyses. Each isotope had to be rastered in succession unlike the electron microprobe which has 5 separate detectors working simultaneously. The maps were taken in the same locations as the individual isotopic measurements done previously. The purpose of mapping

was to observe any relationship between the isotopes over a large area. Pre-sputtering time was kept to a maximum of 120 seconds as these larger rasters removed a lot more material than the individual spot analyses. Deuterium counts were substantially lower than the other isotopes during mapping. In order to map higher counts of D, a significantly longer runtime would be needed and would most likely sputter away much of the jarosite, especially within the mesostasis. Analyzing mesostasis jarosite was an issue for the ion probe because of the low abundance of alteration. This is particularly noticeable when compared to the amount of jarosite material in the larger adjacent veins.

CHAPTER 3: RESULTS

This section will present the results of the application of electron microprobe, synchrotron XRF, and ion probe methods to jarosite in the MIL 03346 meteorite. Jarosite was found in both the MIL 03346 thin sections (,165 and ,190) used in this study. In most instances, the jarosite occurs closer to the edge of the thin section rather than within the center. The following results will focus primarily on two areas of jarosite occurrences within MIL 03346 (one from each thin section). These areas were chosen because jarosite is present in both quantitatively measureable amounts and in various settings.

Terrestrial Jarosite Samples

Electron microprobe and synchrotron XRF were applied to two terrestrial samples of jarosite. Although both the terrestrial samples have hydrothermal origins (supergene), their chemical compositions are different. The Pena Blanca jarosite is homogeneous (Figure 3.1) while the Barranco del Jaroso jarosite shows prominent zoning between Na and K (Figure 3.2a,b). The compositions of the terrestrial jarosites are compared in Table 3.1. Both jarosites show some minor amounts of hydronium substitution. The Na and K concentrations in the Barranco del Jaroso sample alternate along the labeled line of interest in Figure 3.2a.

The Pena Blanca jarosite has mainly K and hydronium in its A-site (~0.94 and ~0.06 atoms per formula unit respectively) and the M-site contained only Fe and minor amounts of Al (~2.87 and ~0.04 apfu respectively). The T-site is occupied solely by SO_4 (~2.02 apfu) and the Z-site was filled with OH^- to exactly

6 apfu. After completely filling the A-site (1 apfu) with hydronium, the recalculated totals for all analyses were close to 100% (> 99.2%). Since the Pena Blanca jarosite is homogeneous, the low totals before the recalculation of the formula unit are due to the H content. The amount of H_2O in this study's Pena Blanca jarosite samples ranges from 11.06-11.28%. This number is consistent with the H_2O content (11.97%) of the Pena Blanca jarosite previously analyzed by Burger et al. (2007).

The same calculations were done on the Barranco del Jaroso jarosite. Results were very similar to the Pena Blanca samples but with a major difference in the A-site of the Barranco del Jaroso samples due to the Na-zoning. In every analysis, the K content contributed a larger portion to the A-site than Na. The largest Na contribution measured was 0.41 apfu (versus 0.53 apfu for K).

Backscattered Electron Image of Pena Blanca Jarosite

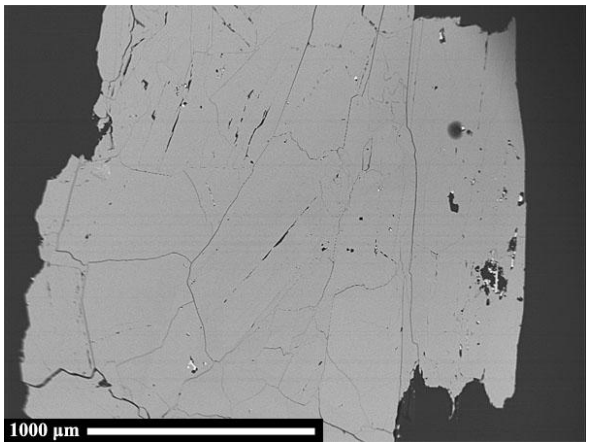

Figure 3.1: *BSE image of Pena Blanca jarosite. The sample is homogeneous K-jarosite.*

Backscattered Electron Images and X-ray Map of Barranco del Jaroso Jarosite

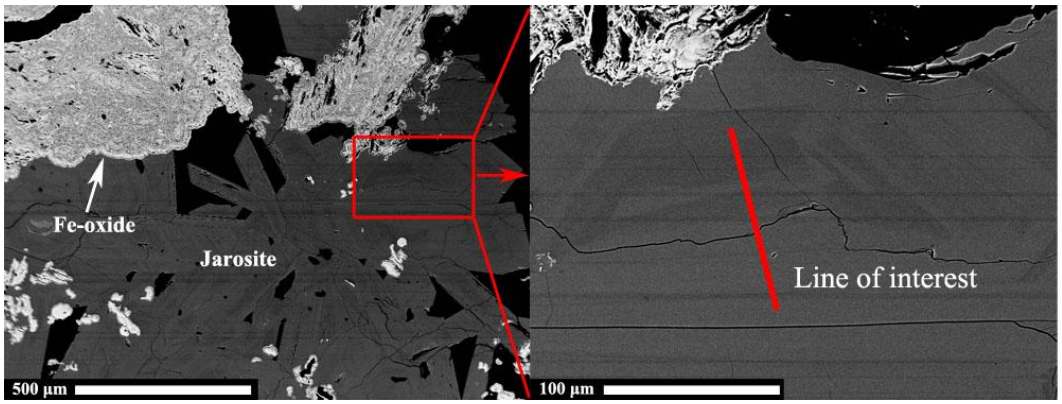

Figure 3.2a: *BSE image of Barranco del Jaroso jarosite, Alternating lighter and darker zones represent zoning between K and Na-jarosites. Bright silver areas near the top of the images are Fe-oxides.*

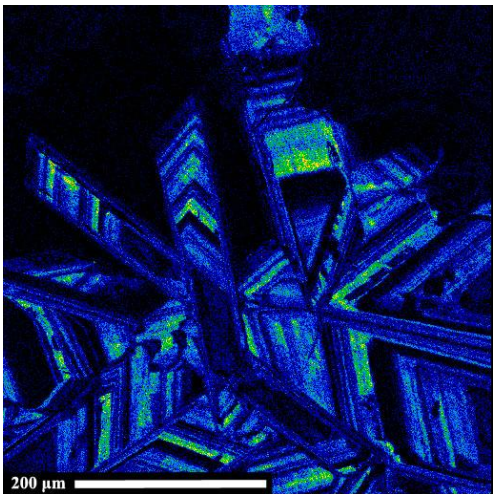

Figure 3.2b: *Na X-ray map of zoned jarosite from Barranco del Jaroso. Brighter areas represent high Na, darker areas represent more K-rich zones.*

Table 3.1 : EPMA Analyses of Terrestrial Jarosites

	Terrestrial Jarosites								
Oxide wt%	**Pena Blanca**			**Barranco del Jaroso**					
K_2O	8.9(1)	9.1(1)	8.9(1)	5.9(1)	5.5(1)	7.9(1)	8.0(1)	8.4(1)	5.11(9)
Na_2O	0	0	0	1.22(7)	2.5(1)	0.71(6)	0.30(4)	0	2.6(1)
Fe_2O_3[a]	46.3(5)	46.1(5)	46.3(5)	47.2(5)	47.8(5)	46.5(5)	47.0(5)	46.4(5)	47.4(5)
Al_2O_3	0.40(3)	0.29(3)	0.37(3)	0.10(2)	0.14(3)	0.18(3)	0.15(3)	0.90(4)	0.05(2)
MgO	0	0	0	0	0	0.01	0	0.02	0
Cr_2O_3	0.1(1)	0.0(1)	0.1(2)	0	0	0	0.14	0	0
MnO	0.0(5)	0.04(5)	0.01(5)	0	0	0	0	0.05(5)	0
SO_3	32.7(5)	32.6(5)	32.8(5)	33.0(5)	33.0(5)	32.9(5)	32.3(5)	33.2(5)	33.4(5)
P_2O_5	0	0.01	0.00	0	0	0	0	0	0
H_2O[b]	11.24	11.06	11.28	12.27	11.23	11.21	11.53	11.96	11.41
SiO_2	0.01(2)	0.01(2)	0	0	0	0	0	0	0
TiO_2	0.01(3)	0.03(3)	0	0	0.01	0	0	0	0
Total[c]	88.4	88.3	88.6	87.5	89.0	88.2	87.9	88.9	88.5
K	0.94	0.96	0.94	0.61	0.57	0.83	0.84	0.86	0.53
Na	0	0	0	0.19	0.39	0.11	0.05	0	0.41
Fe	2.87	2.88	2.87	2.86	2.93	2.88	2.91	2.81	2.89
Al	0.04	0.03	0.04	0.01	0.01	0.02	0.01	0.09	0
Mg	0	0	0	0	0	0	0	0	0
Cr	0	0	0.01	0	0	0	0.01	0	0
Mn	0	0	0	0	0	0	0	0	0
S	2.02	2.03	2.02	2.00	2.02	2.03	2.00	2.00	2.03
P	0	0	0	0	0	0	0	0	0
H[b]	6.19	6.12	6.19	6.60	6.10	6.16	6.33	6.43	6.17
Total[d]	99.7	99.2	99.8	99.7	100.2	99.4	99.4	100.9	100.0
Total Cation	12.06	12.02	12.06	12.27	12.03	12.04	12.15	12.19	12.04

[a] All Fe calculated as Fe_2O_3.

[b] H_2O and H values calculated based on stoichiometry.

[c] Totals not including calculated H_2O component.

[d] Totals including calculated H_2O component.

MIL 03346 Jarosite Occurrences

Locations of Jarosite Occurrences in MIL 03346 Specimens

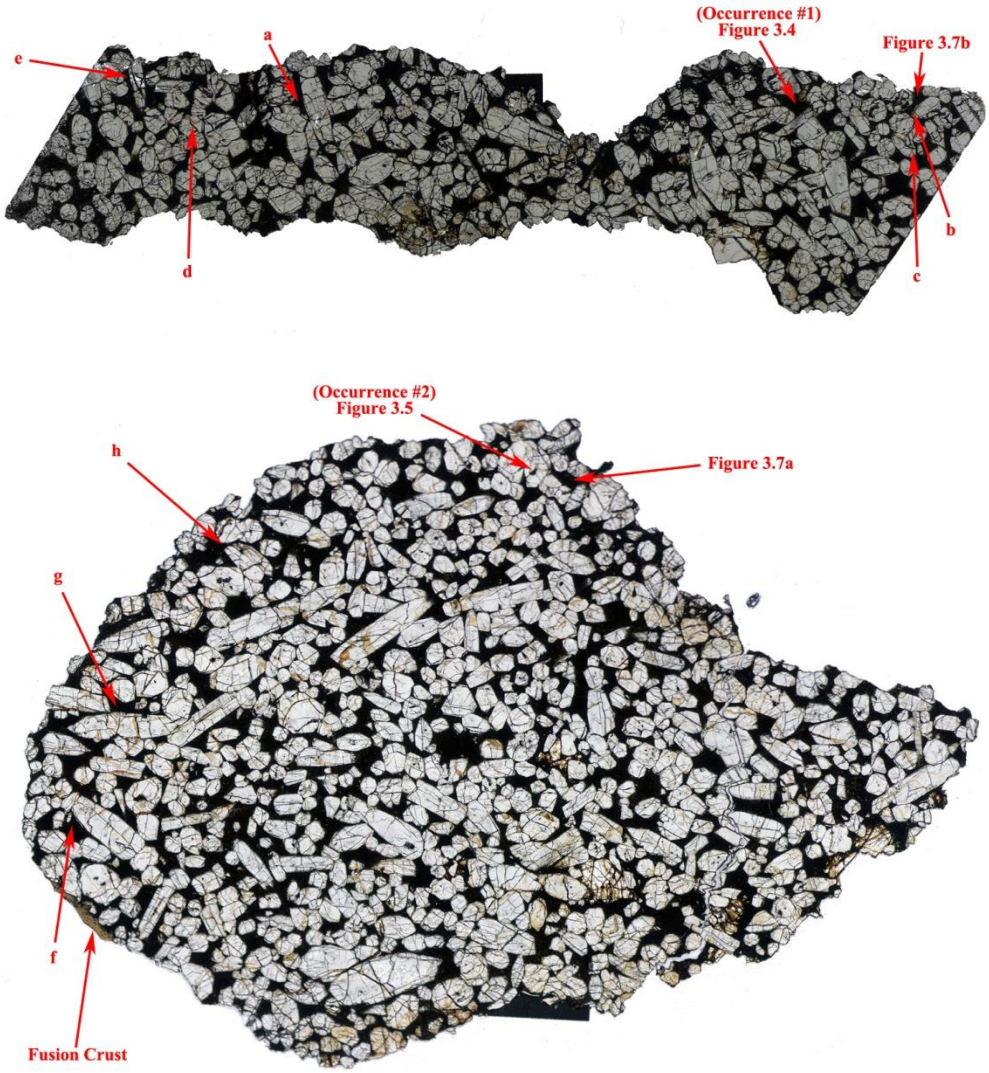

Figure 3.3: *Scans of MIL 03346 ,165 (top) and MIL 03346 ,190 (bottom). Occurrence #1 and Occurrence #2 locations are marked. Fusion crust shown in MIL 03346 ,190. Other occurrences (a-h) shown in Appendix.*

Occurrence #1:

The most representative occurrence of jarosite alteration in the MIL 03346 thin sections is shown in Figure 3.4. This area of MIL 03346, 165 was chosen due to its abundant jarosite alteration over a relatively large area (500x500 um).

Composite Image of Jarosite Occurrence #1

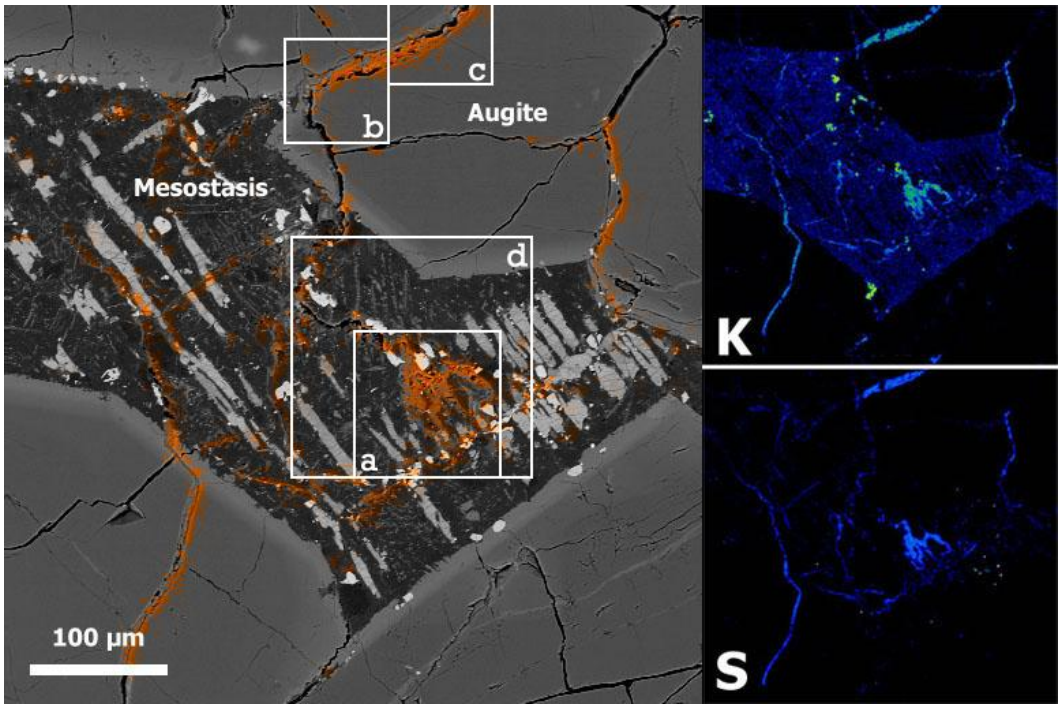

Figure 3.4: *Jarosite (shown in false colour orange) occurrence superimposed onto a BSE image. X-ray maps on the right show abundances of K and S (brighter areas represent higher concentrations).*

The area of interest (Figure 3.4) is located near the edge of the thin section but is not in contact with the any grains touching the sample edge. The area consists of a central pocket of mesostasis surrounded by cumulate augite grains with well-formed edges. Results from X-ray mapping of the area shows that

jarosite occurs in both the mesostasis and veins within the augite. The jarosite occurs most abundantly in one larger vein (areas b and c), represented by the boundary between two separate augite grains. The two smaller veinlets contain only minor traces of jarosite. The majority of the mesostasis jarosite is contained within a 100 x 100 μm area (area a). In this occurrence, the jarosite forms along veins cutting through cumulate grains, which then continue into the mesostasis.

Occurrence #2:

Another occurrence of jarosite was found in an inclusion within a cumulate augite grain in the MIL 03346 ,190 specimen (Figure 3.5). This inclusion is on the opposite side of the section from the fusion crust (Figure 3.3). The inclusion itself is roughly 100 microns in diameter, and contains several phases including pyrrhotite, hematite, K-rich glass, and Ti-Fe oxide (Figure 3.6). The cumulate augite grains in the area, including the grain containing the inclusion, do not contain any abundant alteration products in their cracks (as seen in Figure 3.4). Jarosite occurs along the edge of the inclusion, and covers an area of approximately 15x15 microns (Figure 3.6).

Backscattered Electron Image of Jarosite Occurrence #2

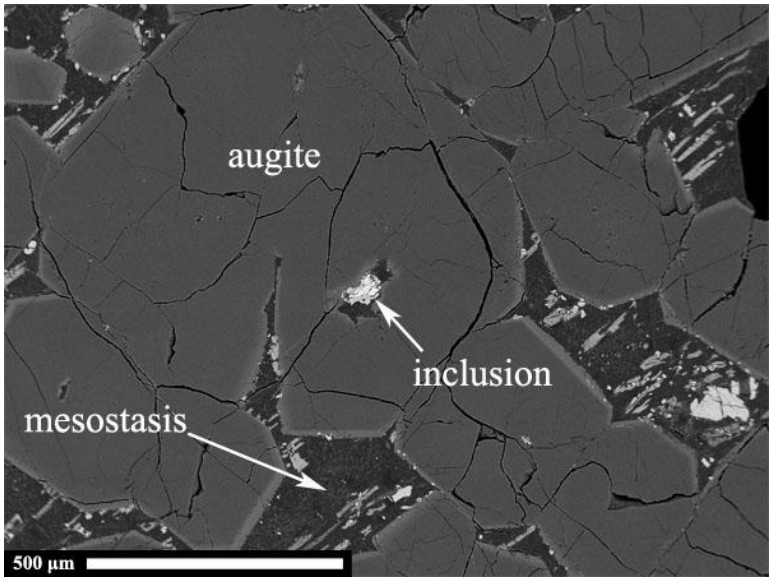

Figure 3.5: *BSE image of the inclusion and the surrounding area within MIL 03346 ,190.*

Inclusion Phases in Jarosite Occurrence #2

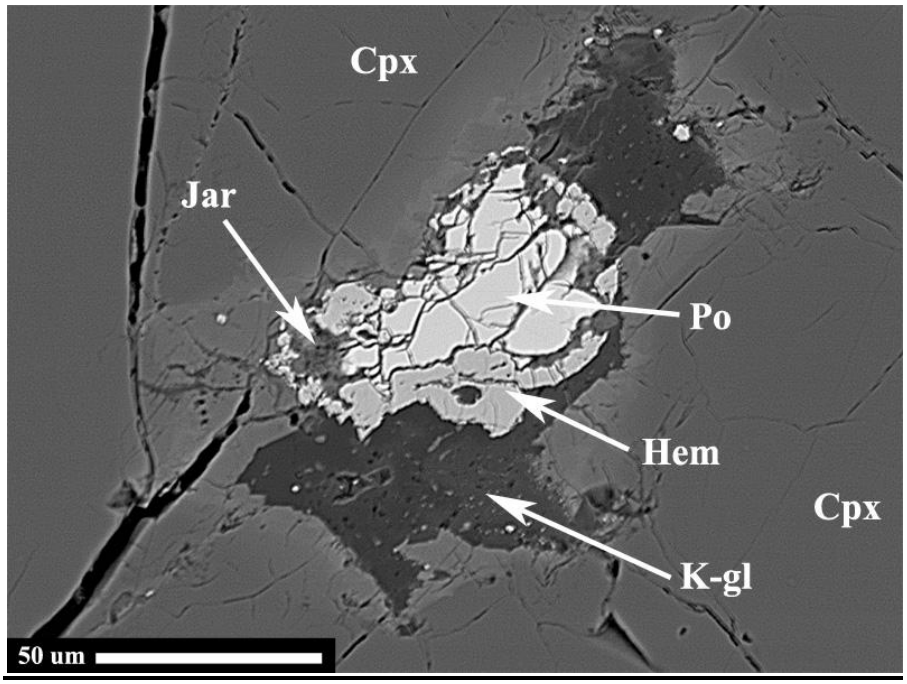

Figure 3.6: *Zoomed in BSE image of the inclusion. Phases include cumulate augite (Cpx), pyrrhotite (Po), hematite (Hem), K-rich glass (K-gl), and jarosite (Jar).*

Other Occcurrences of Jarosite in MIL 03346:

Areas outside of those shown in Figure 3.4 include similar occurrences of jarosite (Appendix, Occurrence a-h). The majority of jarosite found in other areas of the sample occur as veins within the cumulate augite grains. These veins typically run parallel to the edge of the augite grain (Figure 3.7b). Other occurrences (Figure 3.7a) show similar connections between veinlet and mesostasis jarosite in comparison to Occurrence #1.

Composite Images of Other Jarosite Occurrences

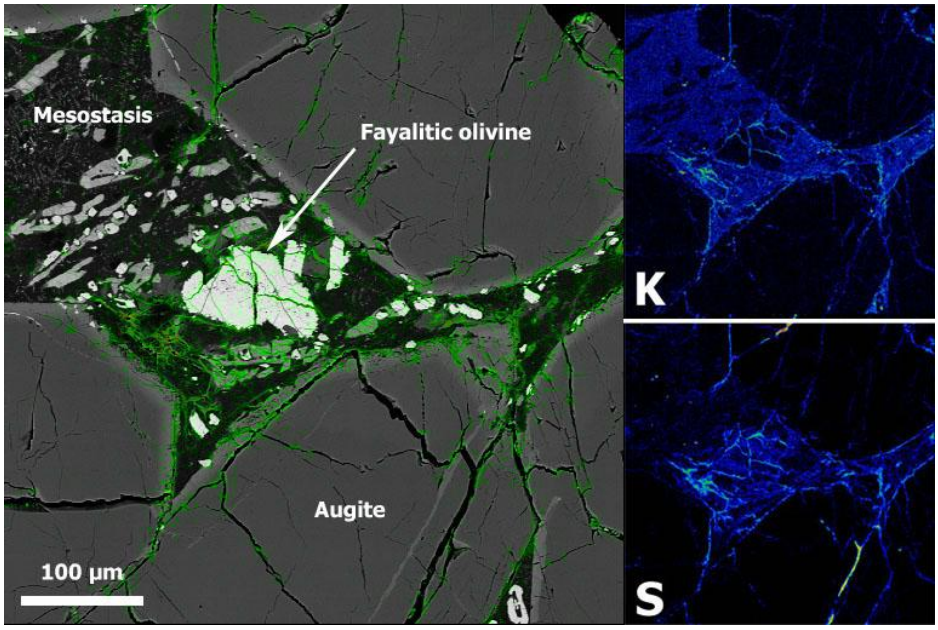

Figure 3.7a: *Jarosite occurrence from MIL 03346 ,165 superimposed onto a BSE image. Jarosite is shown in false colour green. X-ray maps of K and S are shown (inset).*

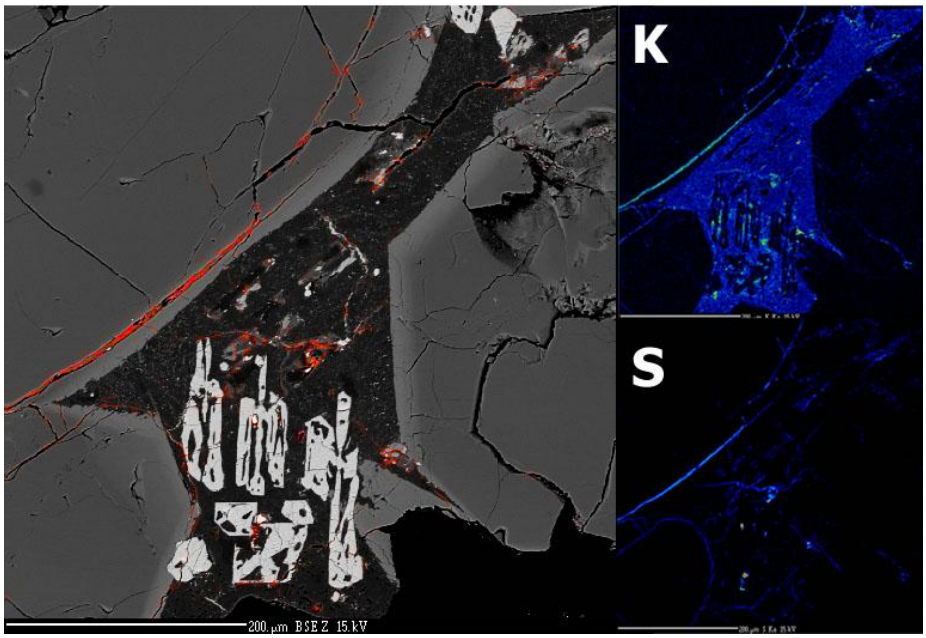

Figure 3.7b: *Jarosite occurrence from MIL 03346 ,165 superimposed onto a BSE image. Jarosite is shown in false colour red. X-ray maps of K and S are shown (inset).*

Figure 3.7a shows an olivine grain within the mesostasis. This area shows only minor amounts of jarosite occurring between the augite grains. These occurrences consist of sub-micron veinlets within cracks in the olivine grain, similar to the occurrence found by Herd (2006). Figure 3.7b shows a similar setting to the vein-filled jarosite in Figure 3.4, but the major difference is that this area has jarosite veins running parallel to the long axis of the augite grain. This jarosite vein extends 200 microns in length.

Quantitative Analysis Results

Occurrence #1:

In the vein jarosite occurrence, the analysis included intergrowth phases which are most likely a mixture of augite and glass (high Fe, Mg and Si but low K and S) due to the proximity and abundance of these phases in the specimen. These phases were linearly subtracted to remove all Si content. The corrected jarosite analysis was calculated using the same ideal formula [$A_1M_3T_2O_8Z_6$]. With the mesostasis jarosite occurrence, the intergrown glass mixture was also subtracted from each analysis to remove all Si content. The results are presented in Table 3.2.

The abundances of the major elemental oxides (K, S, Fe) in the Pena Blanca and MIL03346 samples both represent the K-rich jarosite ($KFe^{3+}_3(SO_4)_2(OH)_6$). Although there is a small amount of Na substitution in the MIL 03346 jarosite occurrences, they do not show the same degree of Na substitution that is observed in the Barranco del Jaroso jarosite. Substantial

hydronium substitution with the K or Na site is also characteristic of the MIL 03346 jarosite in addition to minor PO_4 substitution in the T-site and minor Al substitution in the M-site. After recalculation of the chemical formula, the weight totals for the vein jarosite became very close to 100%.

With the mesostasis jarosite, the quantitative analysis is more difficult to obtain as the alteration is not continuous through the thickness of the thin section. Even after recalculating the formula and completely filling both the A-site and Z-site with hydronium and OH^- respectively, the weight total was only 80.76%. Although the proportions of the major elements in the mesostasis jarosite are similar to the vein jarosite, the low totals show that the mesostasis occurrence is too thin to provide good quantitative results.

Table 3.2 : EPMA Analyses of Occurrence #1

	Occurrence #1 (MIL 03346 ,165)					
Oxide wt%	**Vein Jarosite***	**Vein Jarosite ****	**Vein Cpx/Glass Mix**	**Mesostasis Jarosite***	**Mesostasis Jarosite****	**Mesostasis Glass**
K_2O	5.9(1)	5.9	0.04(1)	4.94(9)	4.71	1.45(5)
Na_2O	0.62(5)	0.62	0.36(4)	0.46(5)	0	4.9(1)
Fe_2O_3[a]	46.3(5)	46.1	24.3(3)	40.5(5)	38.0	15.4(2)
Al_2O_3	1.27(5)	1.26	2.57(7)	3.07(7)	0.40	16.4(2)
MgO	0.14(2)	0.10	7.8(1)	0.12(2)	0.08	0.27(2)
Cr_2O_3	0.1(2)	0.1	0.0(2)	0.0(1)	0.0	0
MnO	0.21(6)	0.21	0.92(8)	0.09(5)	0.06	0.15(6)
SO_3	32.5(5)	32.5	0.07(4)	26.4(4)	26.1	1.7(1)
P_2O_5	0.3(1)	0.3	0.01(1)	0.28(3)	0.24	0.25(3)
H_2O[b]	—	13.05	—	—	11.09	—
SiO_2	0.26(2)	0	48.4(3)	9.0(1)	0	55.5(3)
TiO_2	0.01(3)	0.01	0.65(5)	0.09(3)	0.02	0.42(4)
Total	87.9	100.1	102.3	85.6	80.7	99.3
K	—	0.60	—	—	0.59	—
Na	—	0.10	—	—	0	—
Fe	—	2.75	—	—	2.80	—
Al	—	0.12	—	—	0.05	—
Mg	—	0.01	—	—	0.01	—
Cr	—	0	—	—	0	—
Mn	—	0.01	—	—	0	—
S	—	1.93	—	—	1.92	—
P	—	0.02	—	—	0.02	—
H[b]	—	6.91	—	—	7.24	—
Total Cation	—	12.46	—	—	12.63	—

* Composition of individual raw microprobe analyses of jarosite and other phases.

** Composition of corrected jarosite analyses.

[a] All Fe expressed as Fe_2O_3 for jarosite formula recalculation.

[b] H_2O and H values calculated based on stoichiometry.

Occurrence #2:

Within the inclusion, four distinct phases were found using quantitative analysis (Table 3.3). The sulfide (pyrrhotite) and Ti-Fe oxide phases are common in the MIL 03346 ,190 specimen. The K-rich glass however, appears to be unique to this inclusion. X-ray maps of mesostasis glass in the MIL 03346 ,165 and ,190 specimens show only minor abundances of K.

Since the quantitative analysis in this occurrence also included other intergrown phases, the analysis had to be corrected using the same process done for Occurrence #1 (Table 3.3). In the inclusion jarosite, both a silica and Ti component were present in the initial analysis. First, the Ti was removed by linearly subtracting the Ti-Fe oxide. The silica was then removed by subtracting the K-rich glass, and the resulting jarosite composition was calculated stoichiometrically using the same ideal formula [$A_1M_3T_2O_8Z_6$]. The recalculated jarosite within the inclusion resulted in similar weight totals for all the major elements when compared to the jarosite analyzed in veins of Occurrence #1 (Table 3.2 and 3.3). Both Na and hydronium substitute for K, while Al and PO_4 substitute for Fe and SO_4 respectively.

Although compositionally similar, this occurrence of jarosite within the inclusion is different than the vein jarosite in Occurrence #1. All the phases and materials associated with jarosite precipitation occur within this single inclusion, suggesting a localized environment for jarosite formation. However, this does not exclude the possibility that these phases were formed in place by Antarctic waters; a scenario which will be discussed further in the next chapter. No jarosite

veinlets extend past the area of this inclusion and likewise, no other phases appear to connect to this inclusion from the outside. The inclusion also occurs within a larger augite grain relative to the average augite grain size in MIL 03346.

Table 3.3 : EPMA Analyses of Occurrence #2

	Occurrence #2 (MIL 03346 ,190)				
Oxide wt%	**Inclusion Jarosite***	**Inclusion Jarosite****	**Ti-Fe Oxide**	**K-rich Glass**	**Pyrrhotite**
K_2O	5.6(1)	5.6	0.12(2)	11.6(2)	0.02(1)
Na_2O	0.58(6)	0.57	0.04(4)	0.95(5)	0.01(3)
Fe_2O_3[a]	48.0(6)	44.3	91.4(9)	4.2(1)	60.9(9)[c]
Al_2O_3	1.63(6)	1.50	1.44(6)	15.6(2)	0.03(3)
MgO	0.07(2)	0.06	0.08(2)	0.39(2)	0
Cr_2O_3	0.2(2)	0.2	0.1(1)	0.2(2)	0
MnO	0.06(6)	0.04	0.52(7)	2.39(6)	0
SO_3	33.8(5)	33.7	2.4(1)	0.17(4)	30.8(9)[c]
P_2O_5	0.29(3)	0.28	0	1.69(7)	0.05(2)
H_2O[b]	—	13.54	—	—	
SiO_2	0.30(3)	0.00	0.80(4)	59.1(3)	0.02(2)
TiO_2	0.27(4)	0.00	6.6(1)	—	0.04(4)
Total	91.1	99.7	103.7	98.3	91.9
K	—	0.55	—	—	
Na	—	0.09	—	—	
Fe	—	2.61	—	—	
Al	—	0.14	—	—	
Mg	—	0.01	—	—	
Cr	—	0.01	—	—	
Mn	—	0	—	—	
S	—	1.98	—	—	
P	—	0.02	—	—	
H[b]	—	7.08	—	—	
Total Cation	—	12.49	—	—	

* Composition of individual raw microprobe analyses of jarosite and other phases.

** Composition of corrected jarosite analyses, after removal of Ti-Fe oxide and glass components.

[a] All Fe expressed as Fe_2O_3 for jarosite formula recalculation.

[b] H_2O and H values calculated based on stoichiometry.

[c] Pyrrhotite weight totals represent elemental Fe and S.

Micro-XRF Results

Synchrotron XRF mapping of the MIL 03346 jarosite occurrences show no detectable trace elements of interest. The multivalent elements V, Ce, and Eu, which in previous studies have shown to be able to trace changes in pH and fluid chemistry (Burger 2009), either fall below the limits of the detector or are lost in the noise of the abundant Fe signal (Figure 3.8). XRF maps of K and Fe (Figure 3.9; Box d and Boxes b,c) are consistent with electron microprobe X-ray maps. The main issue with trying to detect any minor elements in the jarosite was caused by the overshadowing Fe signal. Fe, which is very abundant in jarosite, flooded the detector if the shutter was open for long periods of time (greater than 2 seconds). Experimentation with filters and detector positioning did not result in improved data. Moving the detector farther away from the sample did lower the Fe signal but at the cost of lowering all other signals. Moving the detector closer resulted in the detector being flooded. Filters were able to lower the Fe signal to the detector, but were not successful in obtaining any quantitative measurement of minor elements. The implications are discussed further in the next chapter.

Plot of XRF Spectra for Jarosite Occurrence #1

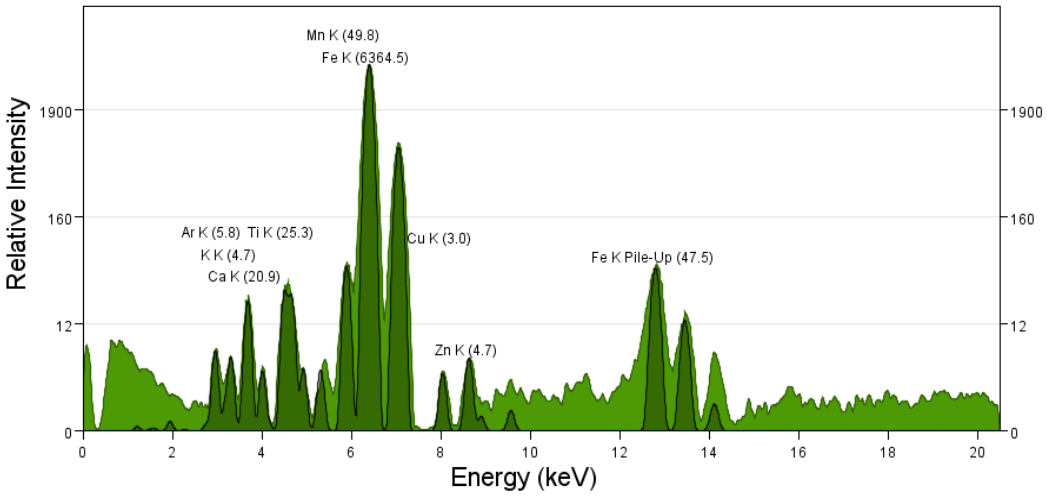

Figure 3.8: *Log scale showing the Fe Kα signal in MIL 03346 jarosite occurrences relative to other detectable elements, obtained by Synchrotron XRF.*

Locating the jarosite with XRF mapping was more difficult than X-ray mapping from the electron microprobe. This is because the K signal was too low to produce to a clear map of the jarosite. As shown on the two XRF maps (d, and b,c in Figure 3.9), only the Fe map was effective in locating the jarosite in the veins. However, the mesostasis jarosite signal is indistinguishable in Fe maps from the abundant titanomagnetite, and without the aid of BSE images, attempting to analyze the jarosite in the mesostasis would have been difficult. The jarosite in the veins did not share this problem because augite grains do not contain as much Fe, especially in their cores.

XRF Maps of Jarosite Occurrence #1

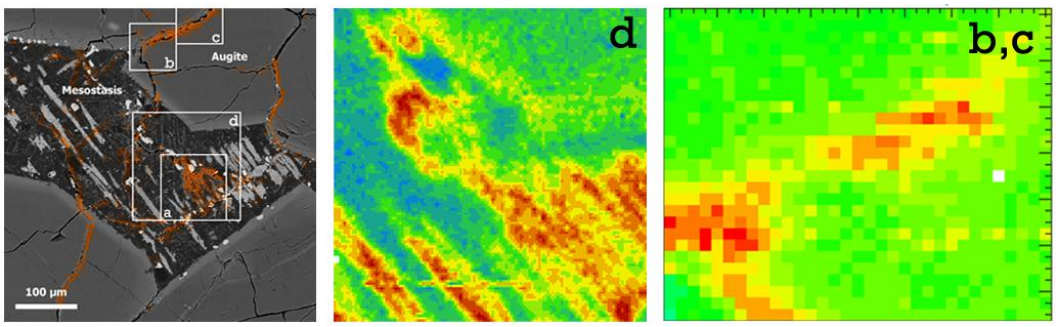

Figure 3.9: *XRF Fe maps of select areas (d and b,c refer to boxes on BSE image in Figure 3.3)*

Ion Probe Results

The main purpose of the ion probe work was to determine whether the jarosite alteration was terrestrial or martian. The H isotopic composition of a terrestrial jarosite (Tintic) was compared to the isotopic composition of hydrogen in the MIL 03346 jarosite. The similarities between hydrogen isotopic measurements of the Tintic and MIL 03346 jarosite occurrences are shown in Table 3.4. Even with a counting time of 10 seconds, the deuterium count rate was very low. Count rates of hydrogen and sulfur were substantially greater than deuterium in all analyses. The d 2H/1H (δD) is calculated from the 2H/1H ratio using the equation:

$$\delta D = 1000 \times \left(\frac{R\text{sample}}{\text{Rstd}} - 1\right)$$

Where $R = \frac{2H\ counts}{1H\ counts}$ and $Rstd = 1.5576 \times 10^{-4}$.

If the jarosite in the meteorite is of martian origin, the δD value would have to be much larger and more consistent with measurements from previous analyses of martian materials. Hydrogen isotopes measured in this study showed that the Occurrence #1 jarosite has a composition consistent with terrestrial jarosite. We measured a similar δD value on the jarosite occurrence found previously by Herd (2006). The MIL 03346 ,190 inclusion jarosite occurrence (Occurrence #2) was not analyzed by ion probe since its discovery came after the ion probe analytical session.

Hydrogen Isotopic Compositions of Tintic and MIL 03346 Jarosite

Table 3.4:

		MIL 03346 Jarosite		
	Tintic Jarosite	**,165 Mesostasis**	**,165 Vein**	**,165 Herd (2006)**
d 2H/1H (‰)	-630.(7)	-669.(7)	-661.(5)	-643.(5)
Elements	***Count Rates (c/s)***			
1H	117242.35	151780.49	172007.15	334592.32
2H	6.85	7.87	9.39	18.67
13C	1176.07	2750.96	3177.25	3236.77
30Si	3.73	5058.09	1967.26	3362.82
34S	183331.4	144401.8	210464.08	329355.88

The δD values of the MIL 03346 and Tintic samples are compared with VSMOW2 and Antarctic water (SLAP2) in Figure 3.10. VSMOW2 and SLAP2 are the newer reference materials for standard mean ocean water and standard

light Antarctic precipitation, replacing VSMOW and SLAP (IAEA 2007). Results from Vicenzi et al. (2007) showing enrichment of jarosite in deuterium are also compared. The measurements of hydrogen isotopes between the mesostasis jarosite and the vein jarosite varied slightly (Table 3.4), but not enough to be outside the range of terrestrial alteration.

Comparison of δD Values of Various Jarosites and Ocean Waters

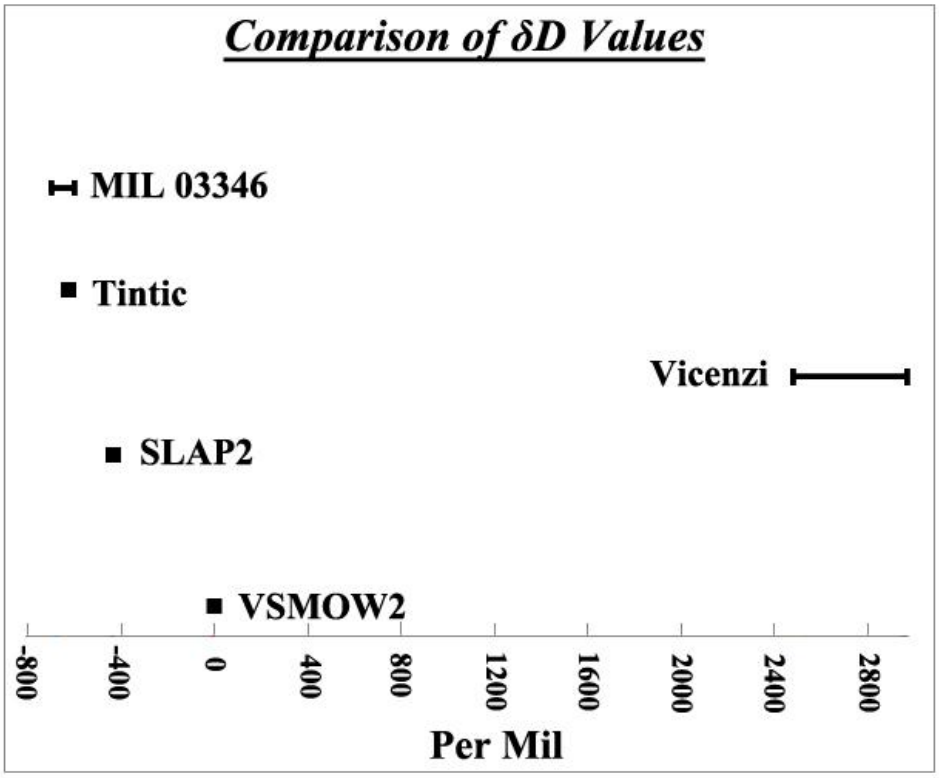

Figure 3.10: *δD values of MIL 03346 and Tintic jarosite measured in this study. "Vicenzi" jarosite δD values from Vicenzi et al. (2007a).*

Ion mapping of hydrogen and sulfur was also done to determine if removal of material from the surface of the sample (unavoidable in ion probe analyses)

could affect the results of the quantitative analysis. Hydrogen and sulfur maps were produced in order to observe the thickness and abundance of the jarosite occurrence (Figure 3.11). The ion maps showed in detail, the extent of jarosite removal from the surface due to the ion beam. The hydrogen map in Figure 3.11a shows only minor amounts of hydrogen in the mesostasis jarosite occurrence, while the count rates of hydrogen in Table 3.4 (earlier analyses) for the same area were similar to sulfur. Conversely, the ion maps of the vein jarosite (Figure 3.11b,c) show similar abundances of hydrogen and sulfur, representing a thicker occurrence of jarosite than seen in the mesostasis. If analyses were done again in the same mesostasis area, the hydrogen count rates would likely be much lower, increasing uncertainties on δD measurements.

Ion Maps of Jarosite Occurrences in MIL 03346 ,165

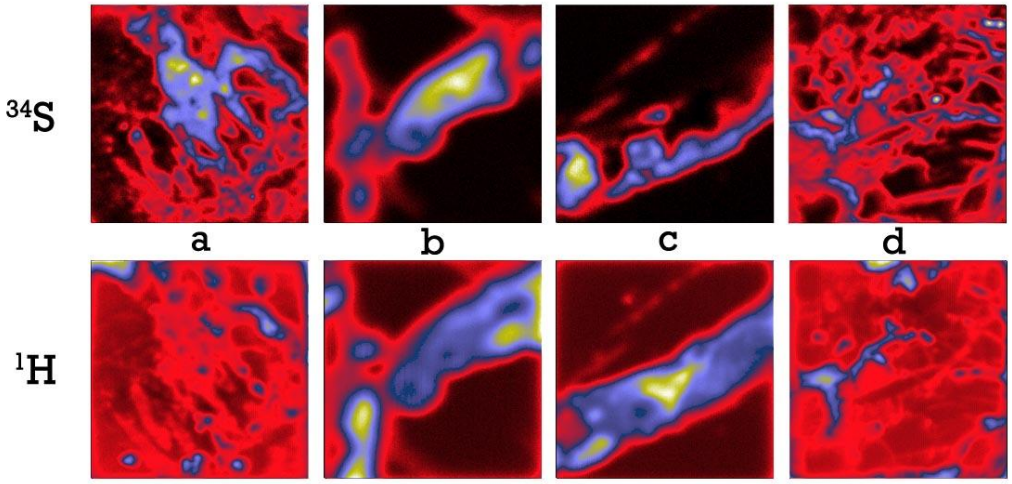

Figure 3.11: *Ion maps of hydrogen and sulfur. Maps were done after the initial isotope data presented in Table 3.3 was collected. Jarosite locations (blue colour) are shown in the sulfur maps.*

CHAPTER 4: DISCUSSION

The initial studies using the electron microprobe showed that the jarosite occurrences in the MIL 03346 specimens are not evenly distributed throughout the sample. The majority of jarosite occurrences are located near the edge of the specimens. The presence of jarosite in the MIL 03346 specimens is not exceedingly rare, but is uncommon given the high amount of iddingsite alteration (rust) within the meteorite. Of the 30 areas of interest that were mapped, only 12 contained evidence of jarosite (Figure 3.1).

An overarching goal of this research was to discover the origin of the jarosite in the MIL 03346 meteorite. EMP, Synchrotron XRF and hydrogen isotopic analyses were used to determine the origin of the jarosite and the effectiveness of each method will be compared in this chapter.

The results indicate two different possible origins for the formation of jarosite in the MIL 03346 meteorite. One scenario, supported by the observations that the jarosite occurrence in the veins is connected to the mesostasis jarosite (Figure 3.3), is that the components required to precipitate jarosite were carried by the waters moving through the rock from outside. The low abundances of K and S in the mesostasis and the network of K- and S-rich veins support the idea that these components were mobilized from outside the local area instead of being derived from local alteration. Another mode of jarosite formation is represented by the inclusion found in MIL 03346 ,190 (Figure 3.5). This jarosite represents a locally-formed occurrence which is supported by the electron microprobe studies of the inclusion. Two lines of evidence support this locally-formed scenario: All

the components necessary for jarosite to form occur within the single inclusion and furthermore, no network of K- and S-rich veins is connected to this inclusion from outside the augite host, at least as observed within the 2-dimensional surface of the thin section. Whether both occurrences are the result of low-temperature alteration or whether the inclusion occurrence is the result of magmatic crystallization is considered and discussed in this chapter.

Origin of the Jarosite in MIL 03346

Two techniques were used to determine the origin of the jarosite in MIL 03346. Synchrotron XRF was used to analyze for trace element compositions with the expectation that the ratios between a set of elements would indicate preterrestrial origins when compared to terrestrial jarosites. The other technique used was hydrogen isotopic analysis using ion microprobe, a method that has proven useful in the past for determining the origin of alteration in other martian meteorites.

Synchrotron Micro-XRF

The use of synchrotron radiation to obtain quantitative XRF trace element data of the martian meteorites was not successful due to the overshadowing Fe signal in the jarosite. The answer to whether the lack of minor element data is the result of the Fe signal or alternatively that the elements of interest are simply not present in the jarosite requires further experimentation.

The Pena Blanca sample which is a homogeneous jarosite did not contain any detectable amounts of the trace elements of interest (V, Ce, and Eu). This

suggests that the fine intergrowth of other phases in the MIL 03346 jarosite occurrences might not be the only reason for the difficulties experienced during minor element data extraction. If the Pena Blanca sample (arguably the best "pure" jarosite specimen in this study) does not contain any detectable trace elements of interest, then detection limits and Fe overshadowing are likely the main causes for the difficulties experienced during synchrotron XRF trace element analyses. The lack of abundant jarosite alteration seen in the MIL 03346 occurrences would therefore be a secondary issue.

Although the goal to obtain quantitative XRF minor element data was unsuccessful, the spot XRF analyses revealed that the jarosite is extremely discontinuous, especially in the mesostasis. Different mineral phases such as the titanomagnetite are closely associated on a micron scale with the mesostasis jarosite. The 3-5 um spot size of the beam detected both jarosite and titanomagnetite simultaneously, indicating a small scale of association between the two separate phases.

The results from the XRF studies show that other phases interfere with the jarosite analyses. If the beam was targeted solely on a spot of jarosite, the K signal should be much larger than what is shown by the data. A larger K signal would then be consistent with the results of the quantitative EMP analyses. The Ca signal in Figure 3.7 can be explained by the the jarosite veins being located within Ca-rich augite grains. Since the distribution of elements detected in Figure 3.7 is a representation of all the spot analyses taken of the jarosite occurrence within the Figure 3.3 area (both in mesostasis and veins), the targeted vein spots

will include some of the signal from neighbouring augite grains and the titanomagnetite intergrowths. This is primarily a beam spot size issue but in the case of the mesostasis jarosite, the low abundance of jarosite is an issue that cannot be resolved even with a smaller beam size.

The physical differences and capabilities between the end stations did not appear to affect the results. Any problems were sample-related as opposed to instrument-based. Both end stations are similar in design as they are both part of insertion devices in a third generation synchrotron. The CLS and APS end stations also used similar instruments for collecting data. Both beamlines used identical Vortex 4 element detectors and similar methods of collection (sample oriented 45 degrees from detector and beam). The results show that the higher energy and therefore higher brightness of the beam at the APS had no effect on the ability to detect the minor elements with any greater success than at the CLS. This part of the study shows that even with the recent advancements in modern synchrotron capabilities, the application of these techniques to analyze jarosite within these martian meteorites is limited.

Ion Microprobe

The results indicate that the jarosite in MIL 03346 ,165 formed on Earth from Antarctic waters that flowed through the rock. Ion microprobe work on the jarosite occurring in this sample showed similar δD values relative to each other in all analyzed areas of interest, including the jarosite occurrence found by Herd (2006). The only variation seen in the H isotopic composition was due to the

sputtering of the ion beam. In the mesostasis jarosite (Figure 3.4, Box a), the low abundances caused the ion count to deteriorate over time. This indicates that the jarosite alteration in the mesostasis is very thin, especially when compared to the neighboring vein (Figure 3.4, Boxes b and c). The thin occurrence of jarosite confirms what was suspected by the micro-XRF analyses; that even a beam spot size of 3 microns has difficulty overcoming the sparse amount of jarosite that occurs in the mesostasis. Although the vein appears to be more resilient than the mesostasis, gaps in jarosite precipitation are shown by the sulfur maps (Figure 3.4 Box c). Deuterium maps were not useful for distinguishing any unique features in the Figure 3.4 area due to deuterium's low count rates. In comparison with the hydrogen maps, the deuterium maps did not show anything distinctive that would necessitate the much longer mapping time required to produce a map of comparable quality.

The larger veinlets (Figure 3.4 Boxes b and c) have more abundant jarosite precipitation with respect to depth than other areas, which is demonstrated by the consistent stream of ions resulting in high count rates. This suggests that fractures in the augite grains provided a more favorable path for fluid flow than the mesostasis, resulting in more precipitation of jarosite. But hydrogen maps (Figure 3.11) show that even the veins of jarosite are discontinuous with voids occupying areas within the vein, requiring careful positioning of the beam for spot analyses. These voids could have resulted from either incomplete precipitation of jarosite within the fractures or removal of material during the sample preparation process, as jarosite is softer than the surrounding augite grains.

Terrestrial Contamination/Mixing

The large variation in δD values within individual meteorites like MIL 03346 suggests that some extent of terrestrial contamination may have occurred. Vicenzi (2007) measured δD values that are well above the range for terrestrial jarosites while the δD values in this study fell within the range for terrestrial waters.

All possible contamination sources related to sample analysis in this study were carefully considered before analyzing the specimens using the various methods. The specimens were always carbon coated under vacuum before being placed into the sample stage of the electron microprobe. When using the ion microprobe, any sorbed water on the thin section surface would have been removed before isotopic analysis by beam presputtering on the area of interest.

A possible source of terrestrial contamination could come from the sample preparation process of the MIL 03346 specimens. All NASA thin sections are prepared using water, although the likelihood of substantial isotopic exchange occurring is low. Kerridge et al. (1988) studied the deuterium exchange during acid-demineralisation of the Murchison meteorite. The samples they used contain organic matter with δD values that are at least 1000‰ greater than the materials used in the lab to prepare them. Their results showed only minor exchange of the H with D, an amount that would not affect the conclusions drawn by the measured δD values. This is because their meteorite material originally had a large enrichment of deuterium, resulting in non-terrestrial δD values even after minor exchange with terrestrial contaminants. If the MIL 03346 ,165 jarosite occurrence

in Figure 3.3 is of martian origin, the δD values would still remain non-terrestrial after the sample preparation, since the δD values measured in other martian meteorites can be up to 4000‰ greater than terrestrial δD values (Watson et al. 1994, Vicenzi et al. 2007a).

Another possible explanation for the large variation in δD values is that if the jarosite formed in Antarctica, terrestrial alteration could produce a wide range of isotopic ratios. Tyra et al. (2007) discovered that terrestrially altered carbonates in Antarctic CM chondrites show $\Delta^{17}O$ values that evolve away from the terrestrial mass fractionation line. This suggests that the low temperature terrestrial alteration through interactions between Antarctic water and the meteorite matrix caused the oxygen isotopic ratio to shift away from terrestrial values. Whether this process could occur with hydrogen isotopic compositions is uncertain.

Alternatively, Rye et al. (1995) performed oxygen and hydrogen isotope fractionation experiments between jarosite and water to determine the dependence of temperature on fractionation factors. Their results indicate that at lower temperatures, the isotopic exchange rate in the aqueous phase is slow relative to the chemical reactions in the experiments. This means that the jarosite would incorporate sulfate which was never in complete equilibrium with the water, resulting in erratic oxygen fractionation factors. At higher temperatures (250°C), the alkali exchange rate (Na-K) catches up with the oxygen isotopic exchange reaction, increasing the likelihood of the reaction being closer to equilibrium. This explains why their 250°C jarosite-water fractionation is inconsistent with lower

temperature values. This could also explain why the δD value in the MIL 03346 jarosite is 200‰ lower than the Antarctic water standard (SLAP2), assuming that the jarosite in the MIL 03346 meteorite is terrestrial and formed on the Antarctic surface at very low temperatures.

Unfortunately even though variations in hydrogen isotopic fractionation occur, the likelihood that these factors could alter the δD value by a few thousand ‰ is low. This would point towards a strong possibility that the jarosite found by Vicenzi et al. (2007a) is actually martian in origin and that the jarosite found in the MIL 03346 ,165 section is terrestrial.

Occurrence #1: Mobilized Jarosite Formation

The main occurrence of jarosite analyzed in this study (Figure 4.1) was found to be terrestrial in origin. The network of K- and S-rich veins connecting with the mesostasis jarosite most likely represents a jarosite in which its components were brought into this local area from proximal sulfide and K-rich phases. Given that the jarosite in this area is terrestrial, Antarctic meteorite weathering and aqueous alteration processes need to be discussed.

The Osawa et al. (2003) study of Antarctic micrometeorites (AMMs) discovered that jarosite (identified by synchrotron X-ray diffraction analysis) occurs in a few of these AMMs. Since the majority of their AMMs were elementally chondritic, the jarosite must have formed on Earth since the requirements for jarosite formation are not found on chondritic parent bodies (high fO_2, H_2O and SO_4^{2-}). In another study, Wentworth et al. (2005) showed that

aqueous alteration processes are active at permanently frozen Antarctic Dry Valley soils. Their SEM studies showed that the weathering features and alteration products in Antarctic Dry Valley soils and martian meteorites are very similar. The Wentworth et al. (2005) study was an analog study for the environment at the surface of Mars, but they did show that aqueous alteration products do occur on the Antarctic surface at very low temperatures.

Location and Composite Image of Jarosite Occurrence #1

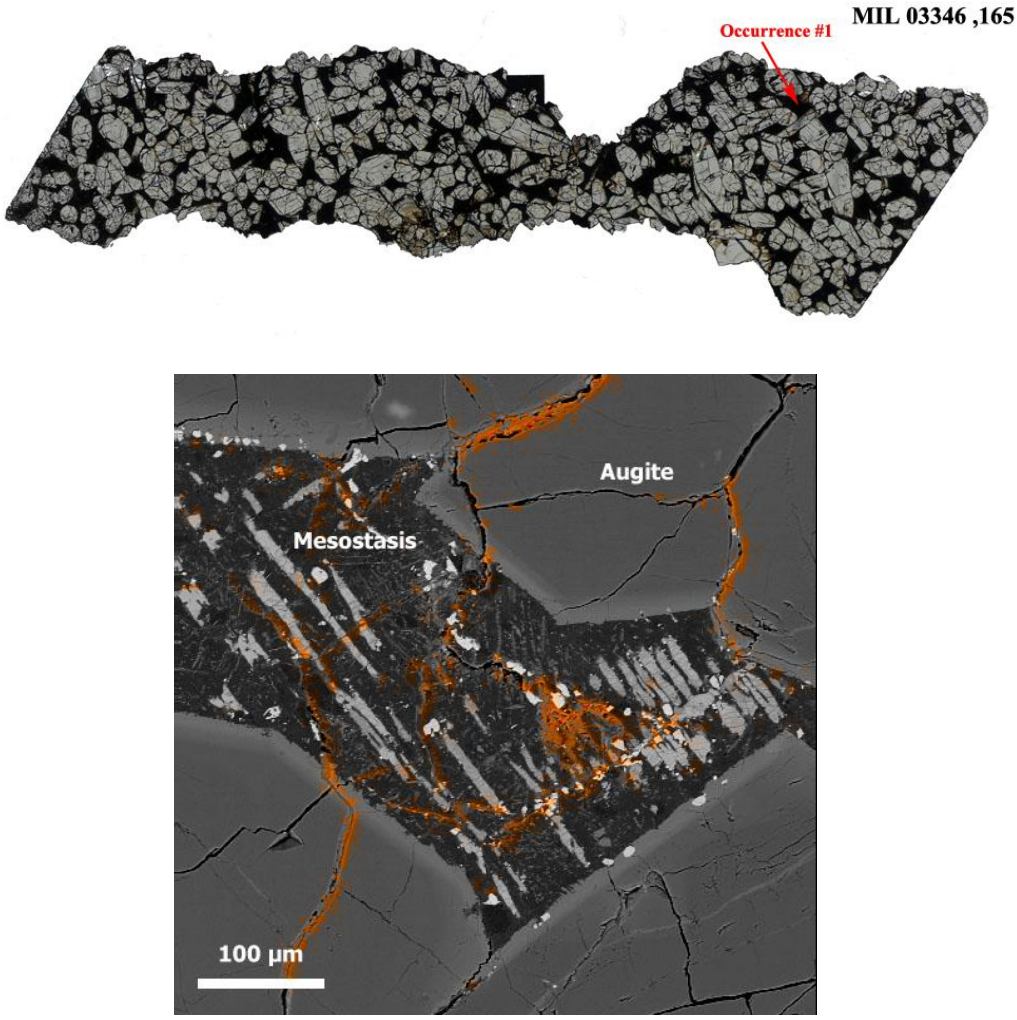

Figure 4.1: *Top: Image of MIL 03346 ,165 (plane light) showing location of Occurrence #1. Bottom: BSE image of a mesostasis/veinlet jarosite (orange) occurrence in MIL 03346 ,165. (This is the same area shown in Figure 3.4)*

There are two possible formation histories for the jarosite occurrence in MIL 03346 mesostasis and veins. Assuming this jarosite began as a martian alteration product, this area could represent a localized area within MIL 03346 that underwent significant hydrogen exchange with the terrestrial waters in Antarctica resulting in the δD values seen in the specimen. This scenario seems

unlikely however, since Vicenzi et al. (2007) found highly elevated δD values in the same meteorite (the longest length of the MIL 03346 meteorite is only 10 cm). That the Antarctic waters only affected this one area of MIL 03346 and not another only a few centimeters away seems highly improbable, especially given the large variations in δD values. The other, more likely possibility is that the jarosite in the mesostasis is solely a terrestrial alteration product, and was not martian jarosite that exchanged with Antarctic waters. This idea is supported by the hydrogen isotopic data and the findings that other Antarctic meteorites exhibit terrestrial aqueous alteration (Osawa et al. 2003, Wentworth et al. 2005). It has been shown from previous studies that at low temperatures, the fractionation factors can vary, but not to the extent of a few thousand ‰. This scenario is further supported by the lack of evidence in this study that shows jarosite being truncated by the fusion crust. The only fusion crust present in two MIL 03346 samples is found in MIL 03346 ,190, but there is no evidence of the fusion crust crosscutting any jarosite occurrences, which would indicate a preterrestrial origin for the jarosite (Figure 4.2).

Locations of Fusion Crust and Jarosite Occurrence #2

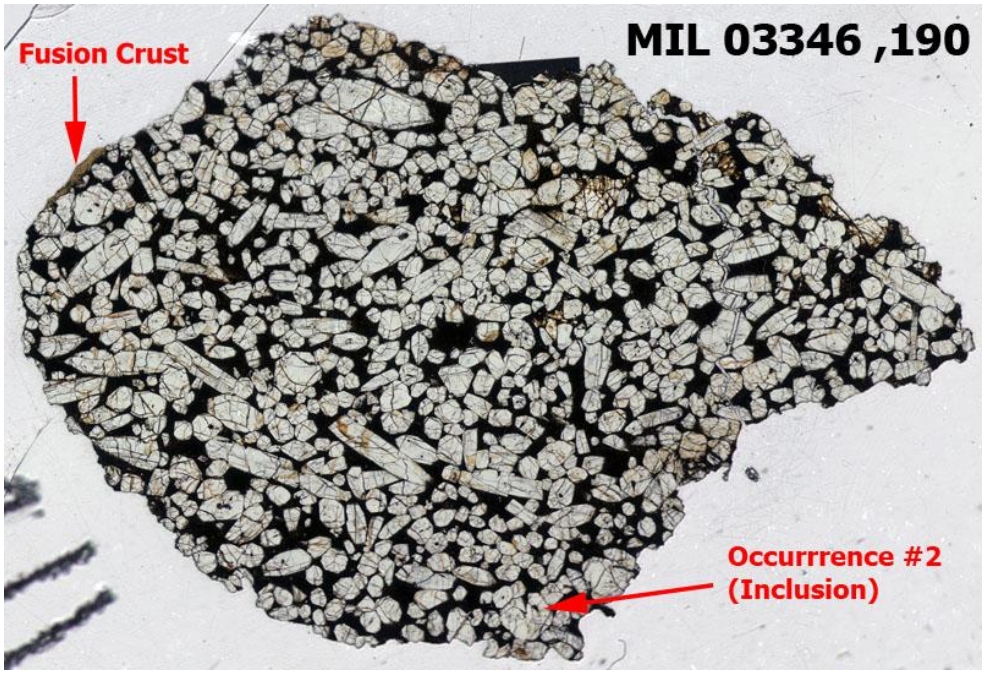

Figure 4.2: *Image of MIL 03346 ,190 (plane light) showing fusion crust on opposite side of the jarosite found in an inclusion (Occurrence #2).*

Occurrence #2: Locally-formed Jarosite

The presence of jarosite in a clinopyroxene-hosted inclusion within the MIL 03346 meteorite is not unique to this study. McCubbin et al. (2009) discovered a melt inclusion that contained jarosite in addition to other phases similar to the ones found in this study (Figure 4.3). Their study reported that the inclusion in their specimen of MIL 03346 had recorded a hydrothermal history that spanned from the magmatic stage into low-temperature aqueous processes, resulting in jarosite precipitation. Their evidence was based on textural relationships and the compositions of the hosted phases characterized by scanning electron microscopy (SEM), Raman-spectroscopy, and electron probe microanalysis.

The inclusion found by McCubbin et al. (2009) is similar to the inclusion found in this study in many ways. The clinopyroxene-hosts for the inclusions are of similar size, both being above the average grain size for MIL 03346. The inclusions themselves are also similar in size, spanning an area roughly 40-50 microns in diameter. The same phases are found in both inclusions, although the inclusion found in this study (Figure 4.4) did not have a clear titanomagnetite phase. Several analyzed Fe-oxide spots did show minor Ti abundances (Table 3.3) but none were as Ti-rich as the areas measured by McCubbin et al. (2009). The abundances of the different phases vary significantly between the two inclusions. The McCubbin et al. (2009) inclusion shows all the phases densely packed together while the one in this study has a large portion of the area occupied by glass. The pyrrhotite grain is also much larger and the hematite phase does not coil as intricately within the inclusion. The hematite in this study's inclusion wraps around one side of the pyrrhotite but terminates at the wall of the inclusion. Nevertheless, the jarosite occurrence in each inclusion is approximately the same size and appears to be texturally similar as well.

The chemical composition of the phases varies between the two inclusions. While the pyrrhotite composition is similar, the composition of the jarosite and the glass is different. The glass occurring in the McCubbin et al. (2009) inclusion is Fe-rich while the glass found in this study's inclusion is K-rich. More importantly, the jarosite in their study contained no hydronium component that would occupy the K and Na site. In the jarosite occurrence in this study's inclusion, there appears to be a significant hydronium component as the K

+ Na components do not completely fill the standard jarosite formula unit (in the best case K + Na = .64 apfu ; Table 3.3).

Images and Phases Contained in McCubbin et al. (2009) Inclusion

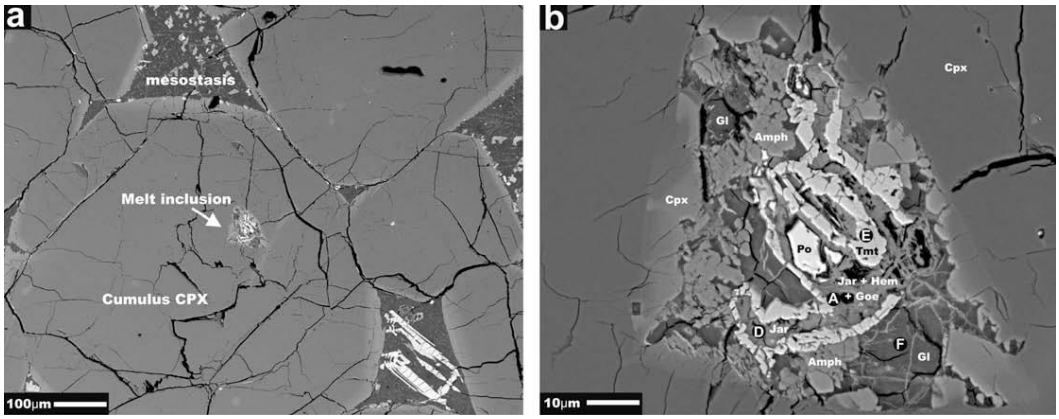

Figure 4.3: *BSE images of a melt inclusion containing jarosite and other phases in MIL 03346 in the study of McCubbin et al. (2009). Phase abbreviations: Jar, jarosite; Tmt, titanomagnetite; Hem, hematite; Goe, goethite; Amph, Cl-rich amphibole; Po, pyrrhotite; Gl, Fe-Si rich glass; and Cpx, clinopyroxene (After McCubbin et al. 2009).*

Images and Phases Contained in Occurrence #2 Inclusion

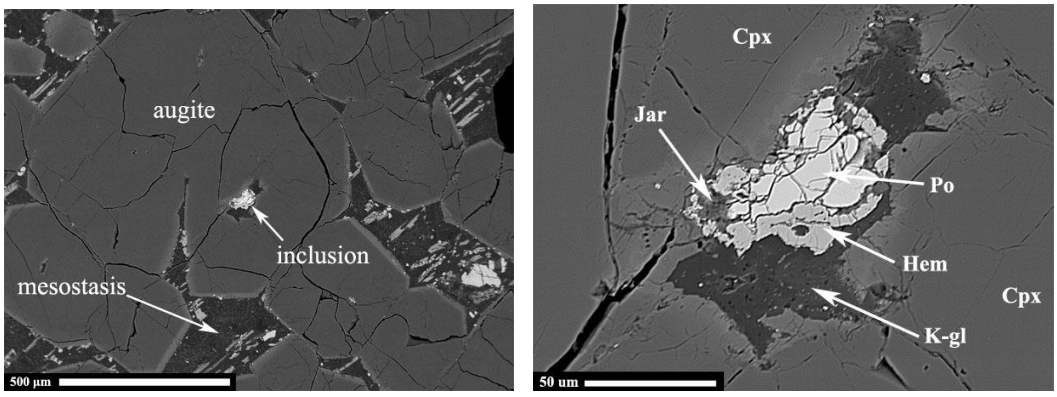

Figure 4.4: *BSE images of an inclusion containing jarosite and other phases in MIL 03346 ,190. Phase abbreviations: Jar, jarosite; Hem, hematite; Po, pyrrhotite; K-gl, K-rich glass; and Cpx, augite. (Same as Figures 3.5 and 3.6)*

McCubbin et al. (2009) concluded that the jarosite they found did represent a hydrothermally precipitated jarosite, which if true, would mean the jarosite is martian in origin. The temperature gradient between the high and low temperature phases needed for their conclusion would not be possible on the Antarctic surface. This does not exclude the possibility of jarosite being formed from solely low temperature processes, which is what the majority of the mesostasis and veinlet jarosite represents. The McCubbin et al. (2009) study demonstrates that the condition for magmatic jarosite existed on Mars during the formation of the MIL 03346 nakhlite host rock. Since there are many similarities both texturally and chemically between their melt inclusion and the one found in this study, and since both occur within the same rock, a comparable process could have also occurred in this newly-found inclusion. However, since the compositions between the two inclusions differ with respect to hydronium substitution, the jarosite in Occurrence #2 could represent a different alteration history. Hydrogen isotopic analysis would be required before conclusively determining if the inclusion jarosite is martian or terrestrial. If the Occurrence #2 jarosite is terrestrial, then its formation was likely due to Antarctic meltwater flowing through and interacting locally with the proximal K-rich glass and sulfide within the inclusion to form jarosite. If the δD value of the jarosite indicates a martian origin, then the differences between the jarosite compositions of Occurrence #2 and McCubbin et al. (2009) could indicate different conditions of growth on Mars.

Regardless of its origin, the presence of jarosite within these inclusions represents the potential for jarosite to precipitate in the mesostasis (Occurrence# 1) and veinlet areas during low temperature aqueous alteration, assuming that some of these melt inclusions were breached at some point after their formation.

How are the Occurrences Related?

If the mesostasis jarosite in the MIL 03346 meteorite originated from one of these breached melt inclusions (assuming the inclusion jarosite is martian), then the precipitation of jarosite in the mesostasis must have occurred in Antarctica and undergone significant hydrogen isotopic exchange with terrestrial waters resulting in terrestrial δD values. This scenario would then be supported by the terrestrial δD values determined in this study for the mesostasis jarosite occurrence (Occurrence #1). However this scenario is not supported by the jarosite compositions in each occurrence. Chemically, the jarosite in Occurrence #1 and Occurrence #2 are similar (Table 3.2 and Table 3.3). Assuming these jarosite occurrences are stable on the Antarctic surface, the possibility that Antarctic waters would remobilize a stable jarosite into another location with similar composition is unlikely.

The other possibility is that the jarosite occurrences in the inclusion, mesostasis, and veinlets are solely due to terrestrial processes as water flowed through the MIL 03346 meteorite. Jarosite precipitation has been shown to occur in other Antarctic meteorites that did not previously contain jarosite (Osawa et al. 2003). This means that the formation of jarosite could instead be a result of

Antarctic surface processes that did not involve the breached melt inclusions; a more likely scenario given how closely the δD values are between the mesostasis jarosite occurrence, the terrestrial jarosite standard, and Antarctic waters (Figure 3.9). This does not exclude the possibility that similar Antarctic alteration processes could have also occurred in-situ within the inclusions themselves (e.g. Occurrence #2) since the components to precipitate jarosite are all located within the inclusion (K-rich glass, sulfides, Fe-oxides). If hydrogen isotopic analysis determines that the jarosite in Occurrence #2 is martian, than the original jarosite would have equilibrated with Antarctic waters to reflect its present composition. If the jarosite is terrestrial, than a similar alteration process would have occurred in both the inclusion and the mesostasis/veinlet jarosite.

The locations of where MIL 03346 ,165 and MIL 03346 ,190 were cut from the original meteorite is shown in Figure 4.5. Both ,165 and ,190 were cut from pieces close to the surface of the rock which is most evident by the fusion crust present in the ,190 section (Figure 4.2). Since both sections analyzed in this study come from near the surface of the MIL 03346 meteorite, there is a strong possibility that these two sections were terrestrially altered by aqueous processes during their residence time on the Antarctic surface.

Possible sequence of events in the MIL 03346 nakhlite's history (modified from Treiman 2005):

1. The MIL 03346 nakhlite is crystallized within a shallow magma chamber beneath the martian surface at ~1.3 Ga. Jarosite is formed in melt inclusions (Occurrence #2).
2. Aqueous alteration at ~0.6 Ga (formation of iddingsite).
3. Ejection from Mars at 11 Ma (Nyquist et al. 2001).
4. Fall to Earth (Antarctica) in recent times. Melt inclusions containing jarosite remain intact and unbreached; e.g. McCubbin et al. (2009) and possibly Occurrence #2.
5. Aqueous alteration on the Antarctic surface from either: a) Terrestrial waters interacting with sulfide and K-rich glass in the rock to precipitate jarosite or b) Remobilization of jarosite from breached melt inclusions (both would result in terrestrial jarosite precipitation within the mesostasis and veinlets along augite grains; e.g. Occurrence #1).

Locations of Thin Sections ,165 and ,190 in MIL 03346

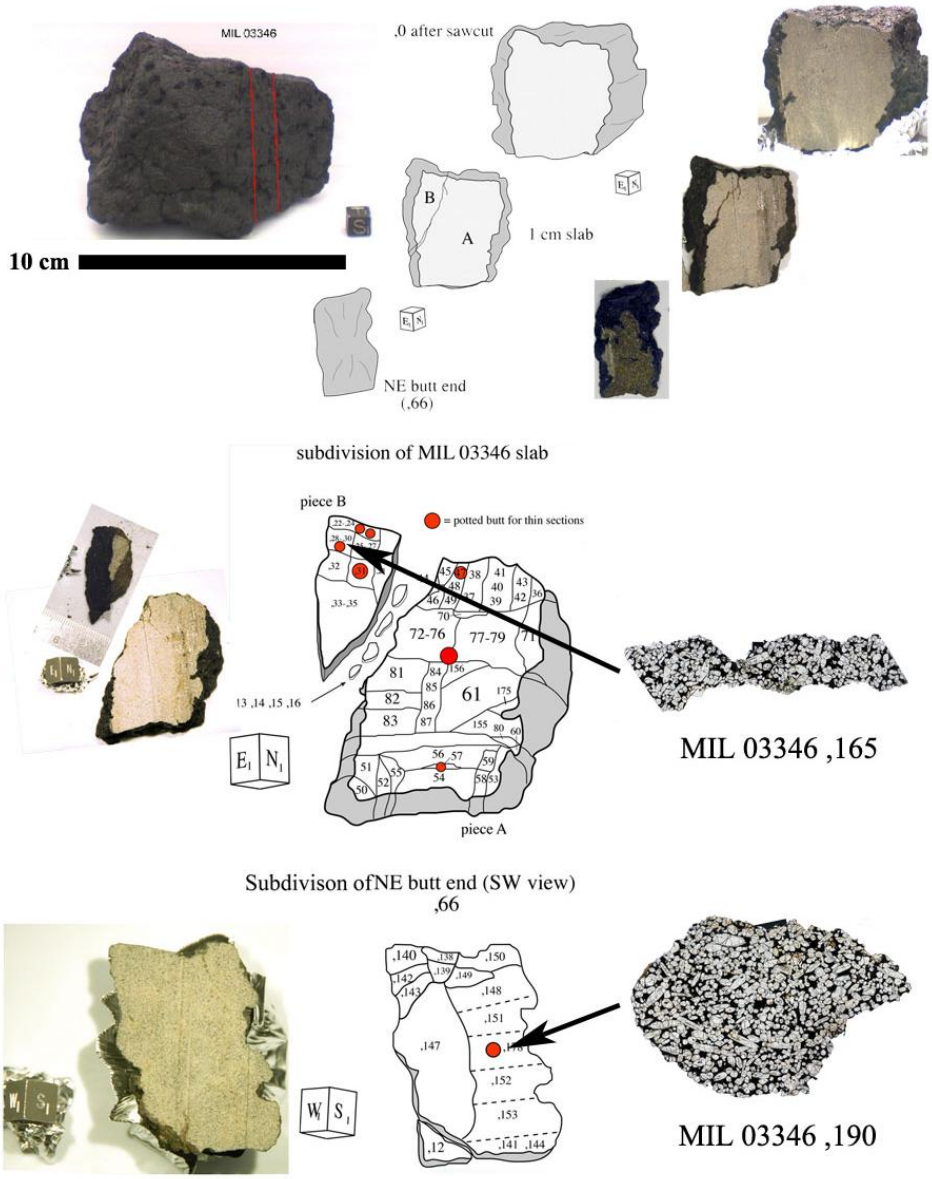

Figure 4.5: *Visual representation of where in the MIL 03346 nakhlite that specimens ,165 and ,190 were cut from (Original images courtesy of Kathleen McBride, NASA 2011).*

Discussion of the Methods

Limitations, Quantitative Analysis Difficulties:

The low abundance of jarosite precipitate for each area of interest in the MIL 03346 specimens was an issue for every method used. The jarosite provided a challenge due to the discontinuous nature and inconsistent thickness of the alteration. This characteristic of the jarosite created difficulties in data collection throughout the study.

In the synchrotron XRF studies, any traces of minor elements are not distinguishable from the background noise and the overshadowing Fe signal. This is true for both the MIL 03346 and Pena Blanca specimens. During the ion probe work, getting consistent measurements of hydrogen isotopes was a challenge in the mesostasis jarosite. Combined with the depleted deuterium signal, this made calculating relative hydrogen ratios difficult. Only the vein-filled jarosite was able to provide reliable data for comparison with the terrestrial jarosite.

When doing quantitative measurements for the jarosite in the MIL 03346 meteorite, only the largest veins of alteration should be considered for dependable data. In the case of MIL 03346 sections ,165 and ,190, the mesostasis jarosite should be used for qualitative analysis only (e.g. X-ray mapping), since quantitative analysis is unreliable due to intergrowths of other phases.

Comparing Effectiveness of Methods:

While one of the goals of this study is to determine the limitations of these methods, the focus on the one particular area within MIL 03346, 165 allowed for

the methods to be compared. When assessing the effectiveness of one method versus another, the purpose for choosing each method must be taken into consideration. Each method used in this study was intended to supplement the other techniques with the goal of collecting as much information about the jarosite in the MIL 03346 nakhlite. No two methods were directly compared on their ability to collect the same data. The only measurement of effectiveness that could be shown by this study would be by evaluating the amount of information that each method provided towards the goals of this research.

The electron microprobe was able to provide the initial qualitative characteristics of the jarosite through X-ray mapping. Quantitative analysis was then able to determine the jarosite chemistry, specifically regarding substitutions of K, Na, and hydronium. The results from the synchrotron XRF analyses did not provide the trace element data that would have attempted to determine the origin of the jarosite using non-destructive methods. The failure to detect trace elements even in the homogeneous terrestrial jarosite (Pena Blanca) could be an indication that this portion of the study was not feasible to begin with. The ion probe work was able to measure the δD values quite consistently. The δD values were able to confirm a terrestrial origin for the jarosite in the MIL 03346 meteorite (Occurrence #1).

Unsurprisingly, the electron microprobe is essential in the analysis of micron-scale alteration products within the MIL 03346 nakhlite and other related meteorites. The electron microprobe also has the advantage of providing quick data collection and easy accessibility. Within this study, there was no technique

used on the electron microprobe that was able to determine the origin of the jarosite. An ion probe was required to make any conclusions regarding its origin. Overall, each successive method used was able to provide new information about the setting of the jarosite.

Improvements and Implications for the Future

The most significant research for the future would be to analyze the hydrogen isotopic composition on all areas of interest, especially in Occurrence #2. The results of this analysis would provide a better understanding of the relation between the inclusion and mesostasis jarosite occurrences in the MIL 03346 meteorite. Synchrotron methods need to be improved in order to analyze micron-scale features. Beamline technology in the future might allow for spot sizes of less than 3 microns which would greatly increase the potential for synchrotron XRF methods to provide reliable quantitative data to either support or expand on the results of electron microprobe analyses. Access to more specimens of MIL 03346, especially from those cut near the center of the meteorite would be very useful. These specimens could have a higher possibility to contain unaltered martian jarosite, as the Antarctic waters would need to percolate deeper into the meteorite. In addition to martian samples, access to other terrestrial jarosites that were supergene-deposited would be more suitable as an analogue for future studies, since the MIL 03346 jarosite occurrences in this study were most likely the result of low temperature Antarctic alteration.

The results of this study could be used for returned samples from Mars. This study's successes and failures with various analytical methods could be helpful in determining the best approach for rocks collected directly from Mars by future sample return missions. Synchrotron methods on these returned rocks would allow for the non-destructive quantitative analyses of the compositions of various phases, assuming the areas of interest are larger than a few microns. If the size of the areas of interest are similar to the ones analyzed in this study, then the use of synchrotron radiation might not be suitable as the problems associated with synchrotron XRF will still be present. The recommended sequence of analyses for the returned samples from Mars would remain unchanged from this study. Electron microprobe is still the most widely available and effective tool for locating and quantitatively analyzing jarosite or any other phase of interest and should therefore be used first. The electron microprobe is able to provide high resolution BSE images and elemental X-ray maps that can be used to guide the rest of the analytical process. Synchrotron radiation methods should then be used if the areas of interest are homogeneous or large enough to be analyzed effectively. Since synchrotron methods are non-destructive, they should always be used before isotopic analyses. Lastly an ion probe should be used to determine the isotopic composition of the areas of interest. Since the returned samples are from Mars, there is no need to use isotopic analyses to determine the origin of a particular phase (assuming that the samples were not contaminated). Instead isotopic data should be used to compare with both terrestrial specimens and martian meteorites.

REFERENCES

Alpers C. N., Rye R. O., Nordstrom D. K., White L. D., and King B. 1992. Chemical, crystallographic and stable isotopic properties of alunite and jarosite from acid-hypersaline Australian lakes. *Chemical Geology* 96:203-226.

Blanchard P. E. R. 2011. Electronic structure of metal pnictides. PhD Thesis University of Alberta (Chemistry), Chapter 2.

Burger P. V., Shearer C. K., Papike J. J., and Karner J. 2007. Trace element crystal chemistry of jarosite: An ion microprobe pilot study (abstract #1985). 38th Lunar and Planetary Science Conference.

Burger P. V., Papike J. J., Shearer C. K., and Karner J. M. 2009. Jarosite growth zoning as a recorder of fluid evolution. *Geochimica et Cosmochimica Acta* 73:3248-3259.

Chevier V., Lorand J., and Sautter V. 2011. Sulfide petrology of four nakhlites: Northwest Africa 817, Northwest Africa 998, Nakhla, and Governador Valadares. *Meteoritics and Planetary Science* 46:769-784.

Clayton R. N., and Mayeda T. K. 1983. Oxygen isotopes in eucrites, shergottites, nakhlites, and chassignites. *Earth and Planetary Science Letters* 62:1-6.

Day J. M. D., Taylor L. A., Floss C., and McSween Jr. H. Y. 2006. Petrology and chemistry of MIL 03346 and its significance in understanding the petrogenesis of nakhlites on Mars. *Meteoritics & Planetary Science* 41:581-606.

Desborough G. A., Smith K. S., Lowers H. A., Swayze G. A., Hammarstrom J. M., Diehl S. F., Leinz R. W., and Driscoll R. L. 2010. Mineralogical and chemical characteristics of some natural jarosites. *Geochimica et Cosmochimica Acta* 74:1041-1056.

Elder F. R., Gurewitsch A. M., Langmuir R. V., and Pollock H. C. 1947. Radiation from electrons in a synchrotron. *Physical Review* 71:829-830.

Fleisher I., Klingelhöfer G., Rull F., Blumers M., Rodionov D., Schröder C., Sansano A., Medina J., Schmanke D., and Maul J. 2008. Sulfate minerals from two Mars analogue sites Rio Tinto and Jaroso Ravine, Spain, investigated by Mössbauer and Raman spectroscopy. *European Planetary Science Congress* 3, A00530.

Goodell, P.C., Lueth, V.W., Peters, L., and Reyes-Cortes, I., 1999. Giant jarosite crystals from the Pena Blanca uranium district, Chihuahua, Mexico. *Mineral Record* 30:85.

Greenwood J. P., Itoh S., Sakamoto N, Vicenzi E. P., and Yurimoto H. 2007. Hydrogen isotope evidence for loss of water from Mars through time. *Geophysical Research Letters* 35, L05203.

Hansteen T. H., Sachs P. M., and Lechtenberg F. 2000. Synchrotron-XRF microprobe analysis of silicate reference standards using fundamental-parameter quantification. *European Journal of Mineralogy* 12:25-31.

Herd, C.D.K. (2006) An occurrence of jarosite in MIL 03346: Implications for conditions of martian aqueous alteration. *Meteoritics and Planetary Science* 41, A74.

Hoefs J. 2004. *Stable Isotope Geochemistry* 5th edition, pp. 244., Springers. Berlin.

Humpris, S.E. 1984. The mobility of rare earth elements in the crust. *Developments in Geochemistry* 2:317-342.

Kerridge J. F., Chang S., and Shipp R. 1988. Deuterium exchange during acid-demineralisation. *Geochimica et Cosmochimica Acta* 52:2251-2255.

Kieffer, H. H., Martin T. Z., Peterfreund, A. R., Jakosky, B. M., Miner E. D., and Palluconi, F. D. 1997. Thermal and albedo mapping of Mars during the Viking primary mission. *Journal of Geophysical Research* 82:4249-4291.

Klingelhöfer G., Morris R. V., Bernhardt B., Schröder C., Rodionov D. S., de Souza Jr. P. A., Yen A., Gellert R., Evlanov E. N., Zubkov B., Foh J., Bonnes U., Kankeleit E., Gütlich P., Ming D. W., Renz F., Wdowiak T., Squyres S. W., and Arvidson R. E. 2004. Jarosite and hematite at Meridiani Planum from Opportunity's Mössbauer spectrometer. *Science* 308:1740-1745.

Kliore, A. J., Cain D. L., Levy G. S., Eshleman V. R., Fijeldbo, G., and Drake F. D. 1965. Occultation experiment: results of the first direct measurement of Mars' atmosphere and ionosphere. *Science* 149:1243-1248.

Lueth V. W., Rye R. O., and Peters L. 2005. "Sour gas" hydrothermal jarosite: ancient to modern acid-sulfate mineralization in the southern Rio Grande Rift. *Chemical Geology* 215:339-360.

Martinez-Frias J., Lunar R., Rodriguez-Losada J. A., Delgado A., and Rull F. 2004. The volcanism-related multistage hydrothermal system of El Jaroso (SE Spain): implications for the exploration of Mars. *Earth Planets Space* 56:5-8.

McCollom T. M., Hynek B. M. 2005. A volcanic environment for bedrock diagenesis at Meridiani Planum on Mars. *Nature* 438:1129-1131.

McCubbin F. M., Tosca N. J., Smirnov A., Nekvasil H., Steele A., Fries M., and Lindsley D. H. 2009. Hydrothermal jarosite and hematite in a pyroxene-hosted melt inclusion in martian meteorite Miller Range (MIL) 03346: Implications for magmatic-hydrothermal fluids on Mars. *Geochimica et Cosmochimica Acta* 73:4907-4917.

McSween Jr. H. Y. 1985. SNC meteorites: Clues to martian petrologic evolution? *Reviews of Geophysics* 23:391-416.

Meyer C. 2006. Introduction to martian meteorites 2006. *Mars Meteorite Compendium*. < http://curator.jsc.nasa.gov/antmet/mmc/Chap%20I.pdf>.

Meyer C. 2008. MIL 03346. *Mars Meteorite Compendium*. <http://curator.jsc.nasa.gov/antmet/mmc/MIL03346e.pdf>.

Misawa K., Shih C.-Y, Wiesmann H., Garrison D. H., Nyquist L. E., and Bogard D. D. 2005. Rb-Sr, Sm-Nd and Ar-Ar isotopic systematic of Antarctic nakhlite Yamato 000593. *Antarctic Meteorite Research* 18:133-151.

Navrotsky A., Forray F. L., and Drouet C. 2005. Jarosite stability on Mars. *Icarus* 176:250-253.

Noguchi T., Nakamura T., Misawa K., Imae N., Aoki T., and Toh S. 2009. Laihunite and jarosite in the Yamato 00 nakhlites: Alteration products on Mars?. *Journal of Geophysical Research* 114: E10004, doi:10.1029/2009JE003364.

Nyquist L. E., Bogard D. D., Shih C.-Y., Greshake A., Stöffler D., and Eugster O. 2001. Ages and geologic histories of martian meteorites. *Space Science Reviews* 96:105-164.

Osawa T., Nakamura T., Nagao K. 2003. Noble gas isotopes and mineral assemblages of Antarctic micrometeorites collected at the meteorite ice field around the Yamato Mountains. *Meteoritics & Planetary Science* 38:1627-1640.

Papike J. J., Karner J. M., and Shearer C. K. 2006. Comparative planetary mineralogy: Implications of martian and terrestrial jarosite. A crystal chemical perspective. *Geochimica et Cosmochimica Acta* 70:1309-1321.

Romanek C. S., Perry E. C., Treiman A. H., Socki R. A., Jones J. J., and Gibson Jr. E. K. 1998. Oxygen isotopic record of silicate alteration in the Shergotty-Nakhla-Chassigny meteorite Lafayette. *Meteoritics and Planetary Science* 33:775-784.

Rull F., Klingelhöfer G., Martinez-Frias J., Fleischer I., Medina J., and Sansano A. 2010. In-situ Raman, Libs and Mössbauer spectroscopy of surface minerals at Jaroso Ravine and related areas in Sierra Almagrera (Almeria-Spain) (abstract #2736). 41st Lunar and Planetary Science Conference.

Rye R. O., and Stoffregen R. E. 1995. Jarosite-water oxygen and hydrogen isotope fractionations: Preliminary experimental data. *Economic Geology* 90:2336-2342.

Shih C.-Y., Nyquist L. E., and Reese Y. 2006. Rb-Sr and Sm-Nd isotopic studies of Antarctic nakhlite MIL 03346 (abstract #1701). 37th Lunar and Planetary Science Conference.

Squyres S. W., and Knoll A. H. 2004. Sedimentary rocks at Meridiani Planum: Origin, diagenesis, and implications for life on Mars. *Earth and Planetary Science Letters* 240:1-10.

Stoffregen R. E. 1993. Stability regions of jarosite and natrojarosite at 150-250 °C. *Geochimica et Cosmochimica Acta* 57:2417.

Swindle T.D., Treiman A. H., Lindstrom D. J., Burkland M. K., Cohen B. A., Grier J. A., Li B., and Olson E. K. 2000. Noble gases in iddingsite from the Lafayette meteorite: Evidence for liquid water on Mars in the last few hundred million years. *Meteoritics & Planetary Science* 35:107-115.

Treiman, A.H., Barrett R. A., and Gooding J. L. 1993. Preterrestrial aqueous alteration of the Lafayette (SNC) meteorite. *Meteoritics* 28:86-97.

Treiman A. H., Gleason J. D., Bogard D. D. 2000. The SNC meteorites are from Mars. *Planetary and Space Science* 48:1213-1230.

Treiman A. H. 2005. The nakhlite meteorites: Augite-rich igneous rocks from Mars. *Chemie der Erde* 65:203-270.

Tyra M. A., Farquhar J., Wing B. A., Benedix G. K., Jull A. J. T., Jackson T., and Thiemans M. H. 2007. Terrestrial alteration of carbonate in a suite of Antarctic CM chondrites: Evidence from oxygen and carbon isotopes. *Geochimica et Cosmochimica Acta* 71:782-795.

Vicenzi E. P., Fries M., Fahey A., Rost D., Greenwood J. P., and Steele A. 2007a. Evidence for young jarosite precipitation on Mars (abstract #5293). 70th Annual Meteoritical Society Meeting.

Vicenzi E. P., Fries M., Fahey A., Rost D., Greenwood J. P., and Steele A. 2007b. Detailed elemental, mineralogical, and isotopic examination of jarosite in martian meteorite MIL 03346 (abstract #2335). 38th Lunar and Planetary Science Conference.

Watson L. L., Hutcheon I. D., Epstein S., and Stolper E. M. 1994. Water on Mars: Clues from deuterium/hydrogen water contents of hydrous phases in SNC meteorites. *Science* 265:86-90.

Wentworth S. J., Gibson E. K., Velbel M. A., and McKay D. S. 2005. Antarctic Dry Valleys and indigenous weathering in Mars meteorites: Implications for water on Mars. *Icarus* 174:383-395.

APPENDIX

Other occurrences of jarosite in MIL 03346:

MIL 03346 ,165:

MIL 03346 ,190:

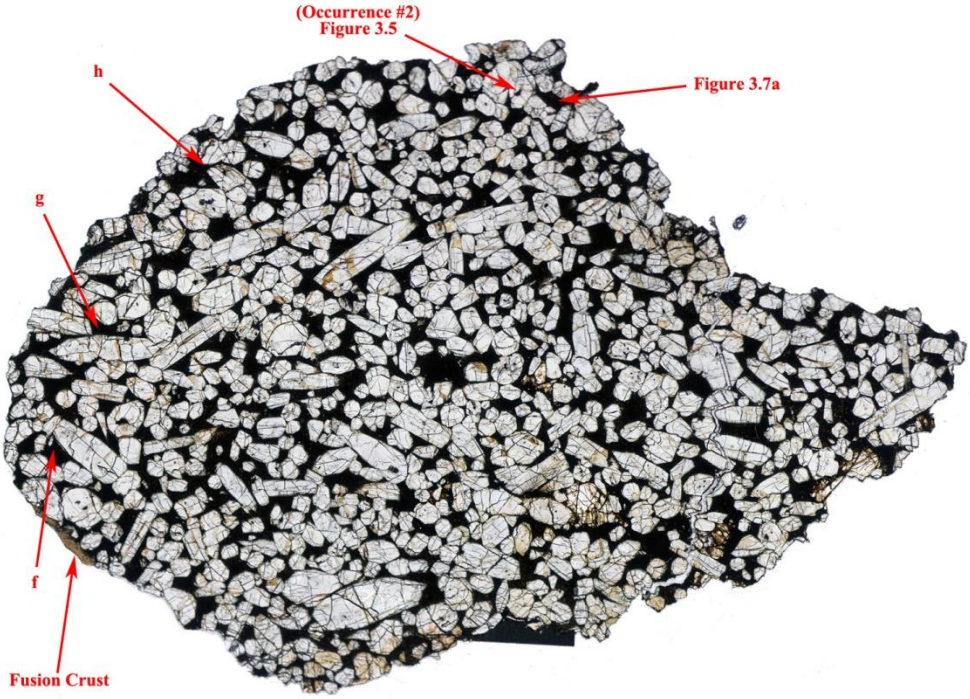

Each occurrence has 1 BSE image and 3 elemental X-ray maps locating the jarosite (Fe, K, S).

MIL 03346 ,165

Occurrence a:

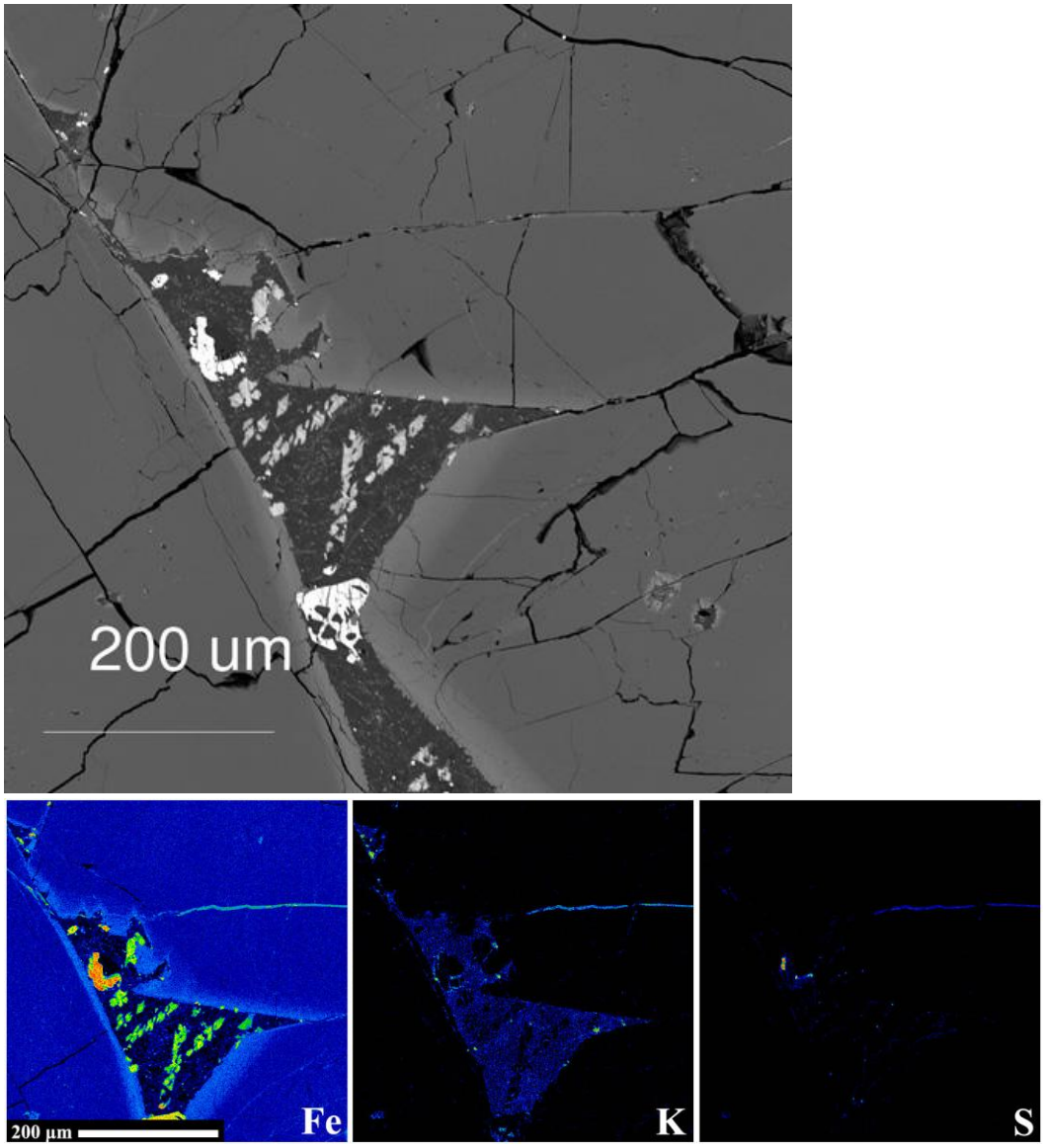

Occurrence b:

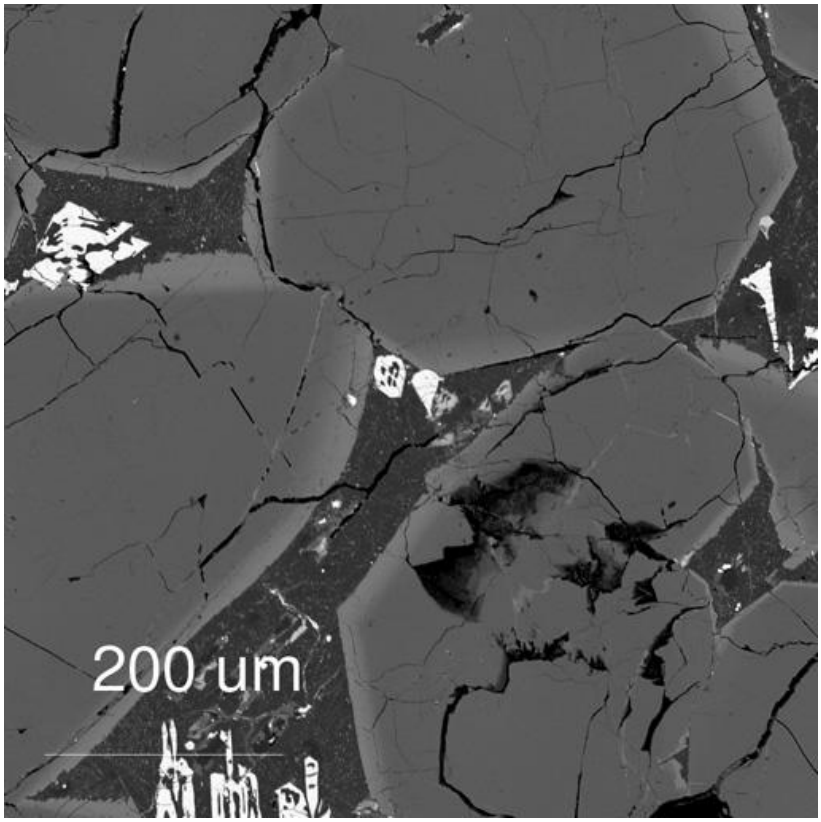

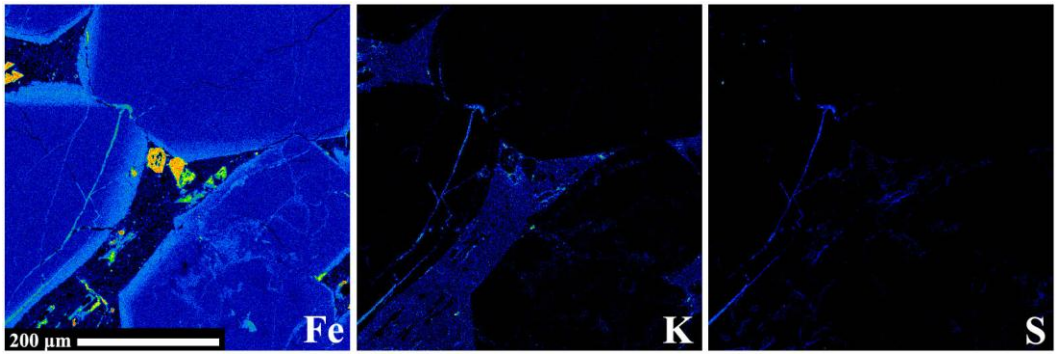

Occurrence c:

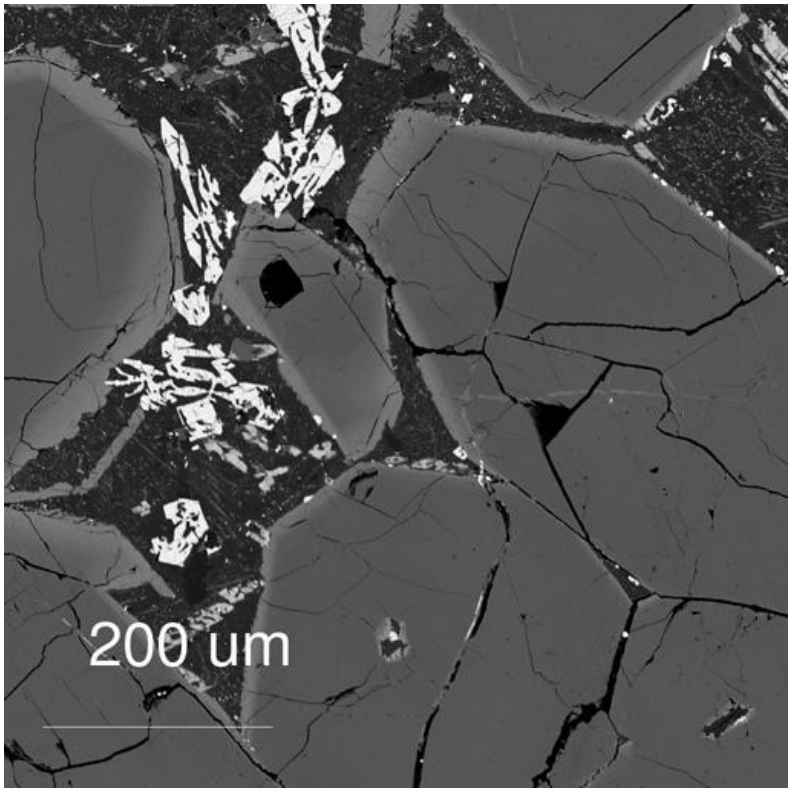

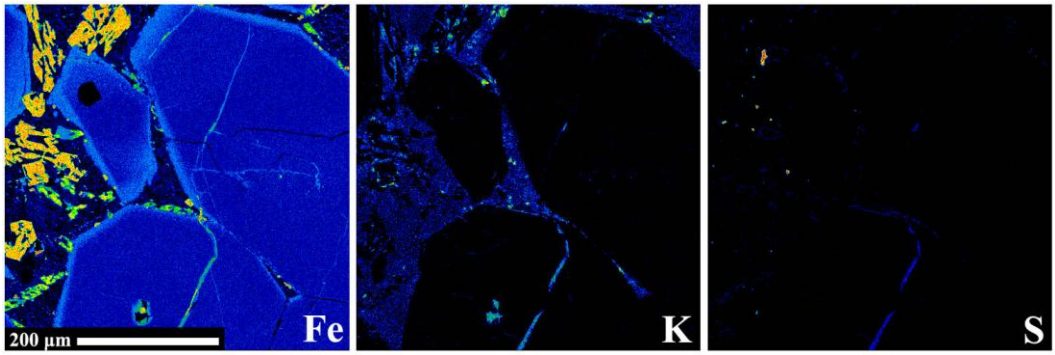

Occurrence d:

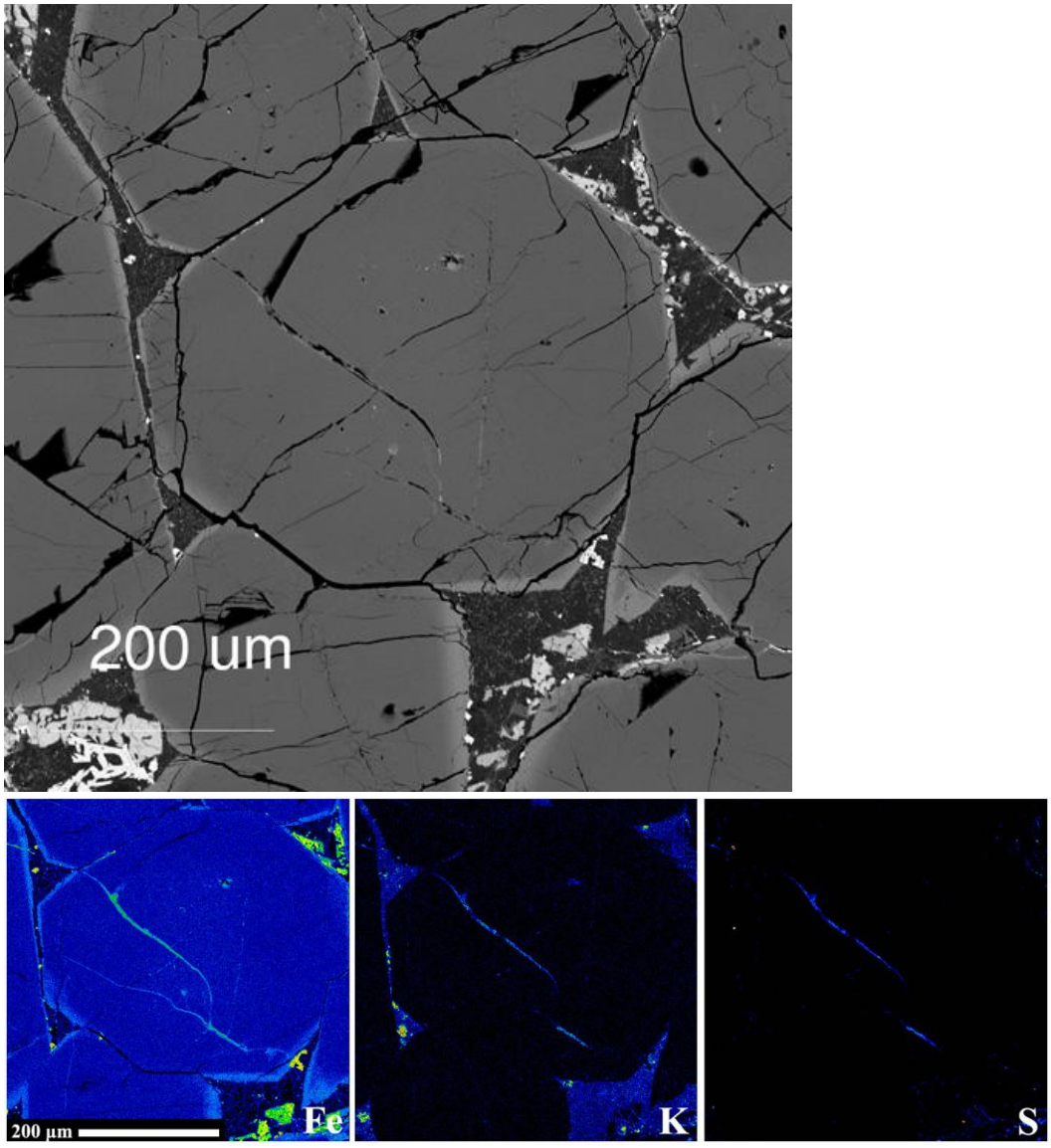

Occurrence e:

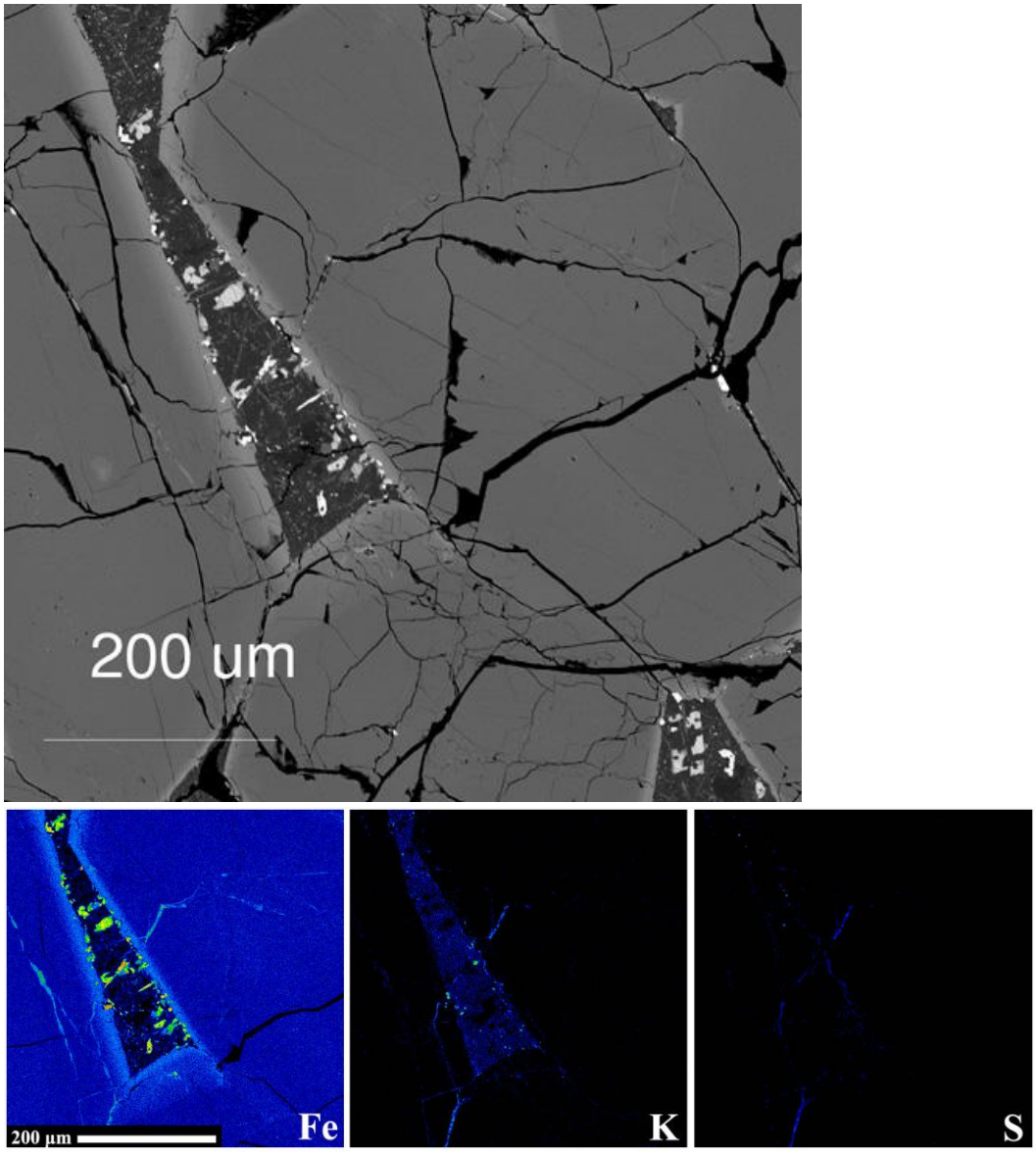

MIL 03346 ,190

Occurrence f:

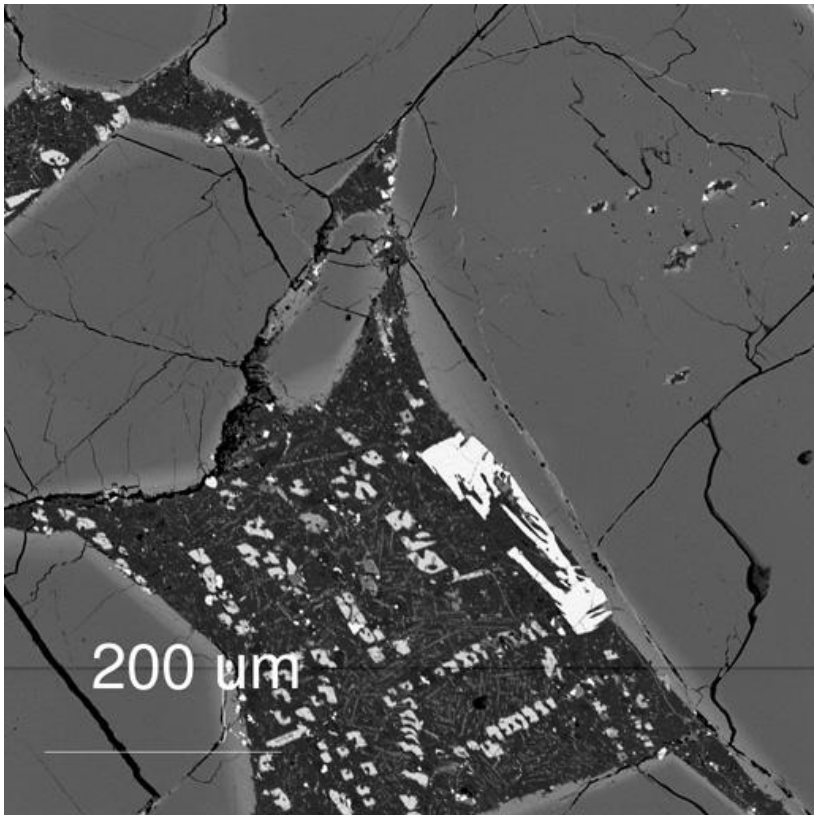

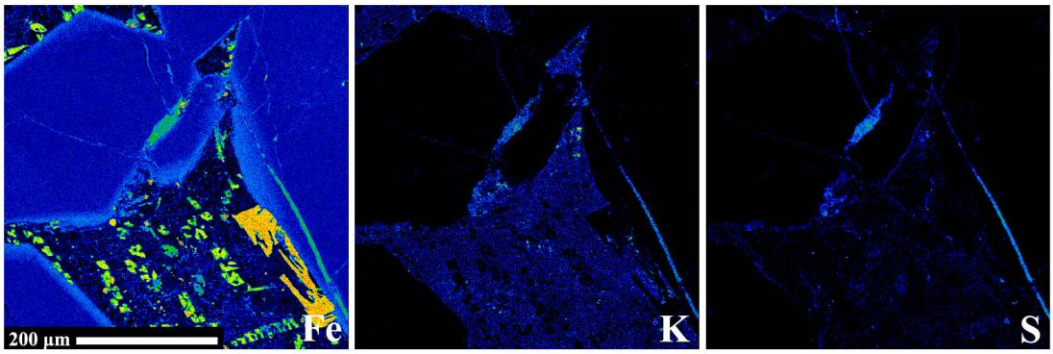

Occurrence g:

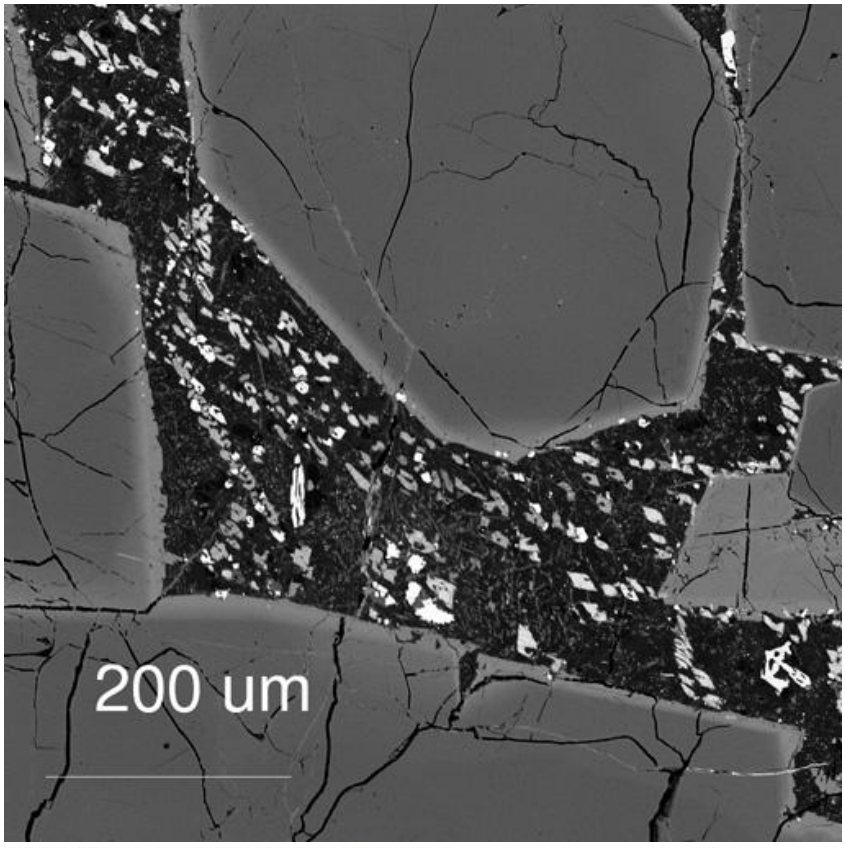

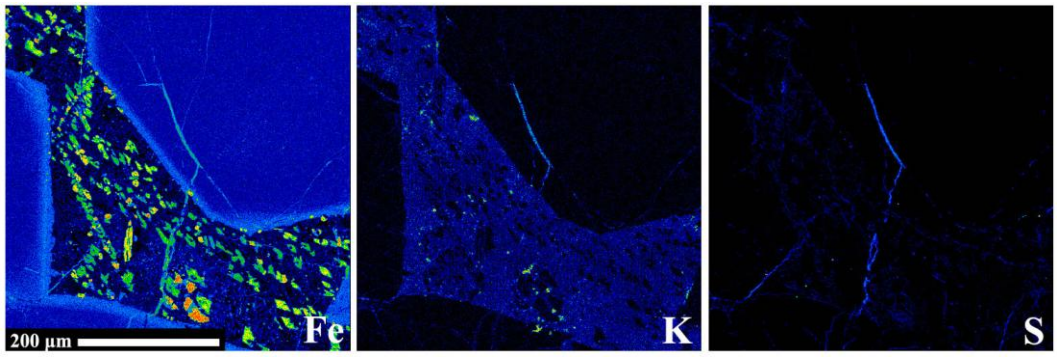

Occurrence h:

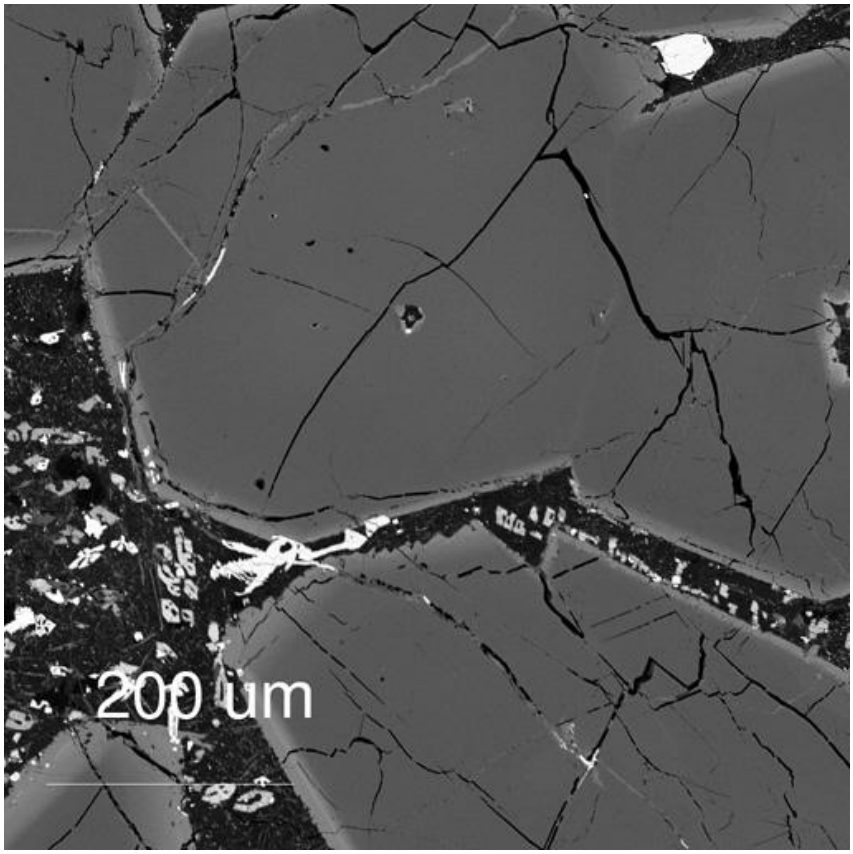

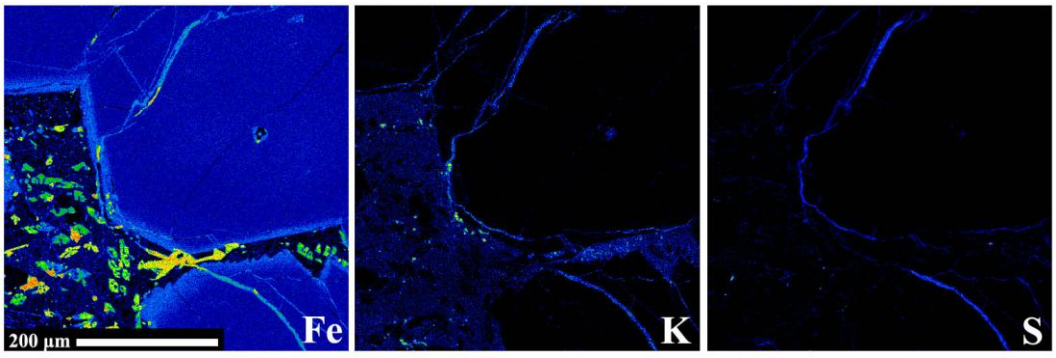

BSE Images of the Terrestrial Jarosites

Pena Blanca:

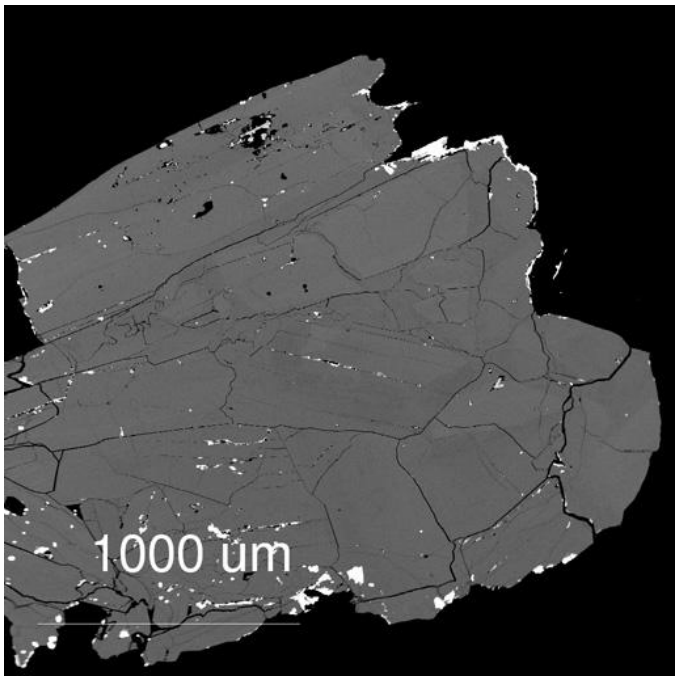

Barranco del Jaroso:

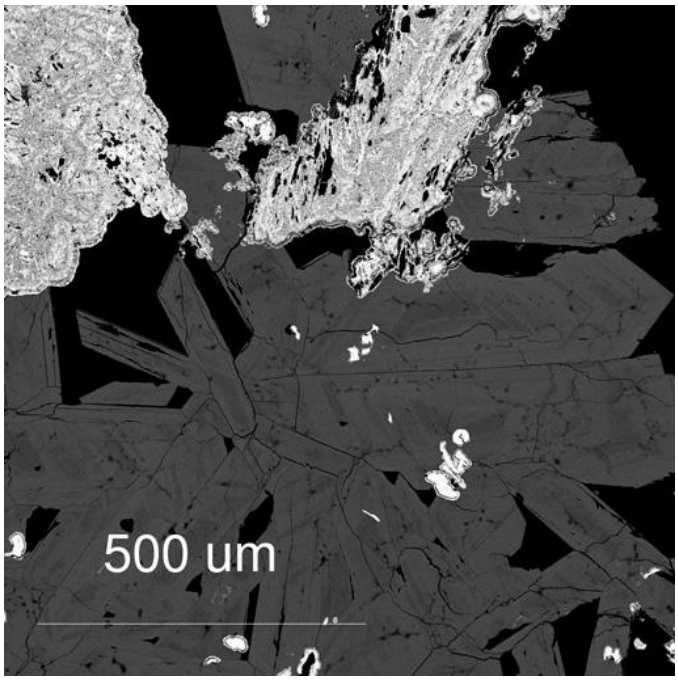

MIL 03346 ,190 Occurrence #2 Supplement

BSE image of Occurrence #2 and coloured image below (brighter areas represent higher Fe content):

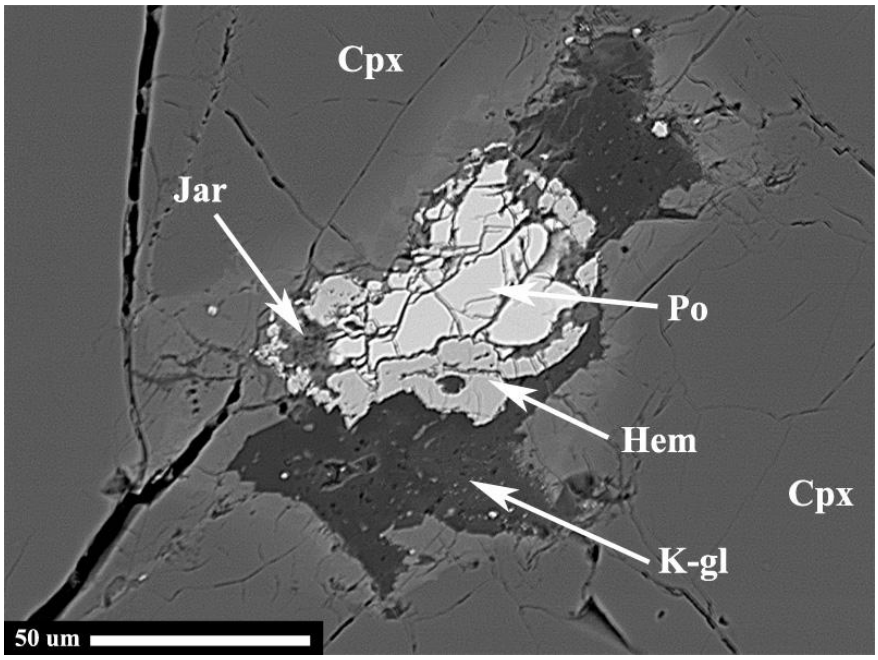

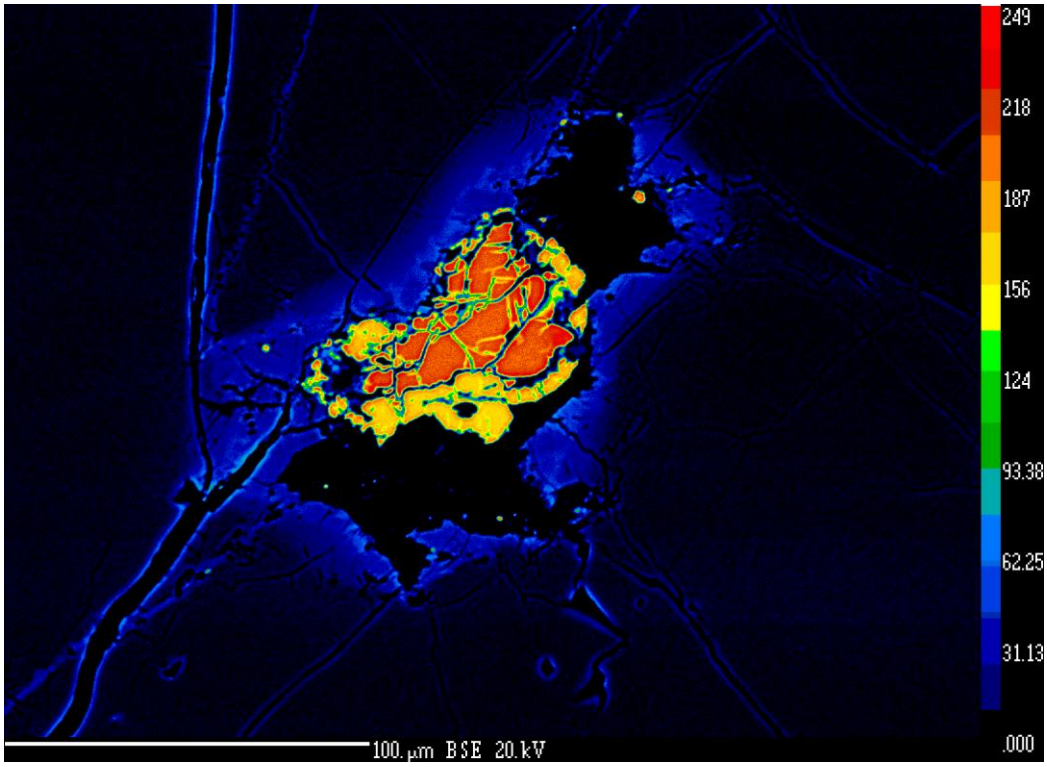

Isotopic Analysis Data

Tintic Jarosite

Elements	*Masses*	*Counting Time (s)*	*Detector*	*Count Rates (c/s)*
1H	1.007825	1	EM	117242.35
2H	2.014000	10	EM	6.85
13C	13.003355	1	EM	1176.07
30Si	29.973770	1	EM	3.73
34S	33.967866	1	EM	183331.4

	d 2H/1H	*STDEV*	*2H/1H*	*STDEV*
Average over blocks:	-627.26	23.816	5.806E-05	3.710E-06
Average over data:	-626.722	45.969	5.814E-05	7.160E-06
Wmean and Error	-629.921	6.635	5.760E-05	1.033E-06

MIL 03346 ,165 Mesostasis Jarosite

Elements	*Masses*	*Counting Time (s)*	*Detector*	*Count Rates (c/s)*
1H	1.007825	1	EM	151780.49
2H	2.014000	10	EM	7.87
13C	13.003355	1	EM	2750.96
30Si	29.973770	1	EM	5058.09
34S	33.967866	1	EM	144401.8

	d 2H/1H	*STDEV*	*2H/1H*	*STDEV*
Average over blocks:	-665.231	29.951	5.214E-05	4.665E-06
Average over data:	-665.231	47.531	5.214E-05	7.403E-06
Wmean and Error	-668.529	6.722	5.163E-05	1.047E-06

MIL 03346 ,165 Vein Jarosite

Elements	*Masses*	*Counting Time (s)*	*Detector*	*Count Rates (c/s)*
1H	1.007825	1	EM	172007.15
2H	2.014000	10	EM	9.39
13C	13.003355	1	EM	3177.25
30Si	29.973770	1	EM	1967.26
34S	33.967866	1	EM	210464.08

	d 2H/1H	*STDEV*	*2H/1H*	*STDEV*
Average over blocks:	-653.621	15.119	5.395E-05	2.355E-06
Average over data:	-652.575	35.091	5.411E-05	5.466E-06
Wmean and Error	-660.886	5.119	5.282E-05	7.973E-07

MIL 03346 ,165 Herd (2006)

Elements	*Masses*	*Counting Time (s)*	*Detector*	*Count Rates (c/s)*
1H	1.007825	1	EM	334592.32
2H	2.014000	10	EM	18.67
13C	13.003355	1	EM	3236.77
30Si	29.973770	1	EM	3362.82
34S	33.967866	1	EM	329355.88

	d 2H/1H	*STDEV*	*2H/1H*	*STDEV*
Average over blocks:	-642.799	25.891	5.564E-05	4.033E-06
Average over data:	-646.907	33.890	5.500E-05	5.279E-06
Wmean and Error	-642.852	4.943	5.563E-05	7.700E-07